UPPSALA
UNIVERSITET

Digital Comprehensive Summaries of Uppsala Dissertations from the Faculty of Science and Technology 1409

Towards Mixed Molecular Layers for Dye-Sensitized Solar Cells

A Photoelectron Spectroscopy Study

JOHAN OSCARSSON

ACTA
UNIVERSITATIS
UPSALIENSIS
UPPSALA
2016

ISSN 1651-6214
ISBN 978-91-554-9664-7
urn:nbn:se:uu:diva-301164

Dissertation presented at Uppsala University to be publicly examined in Häggsalen, Ångströmlaboratoriet, Lägerhyddsvägen 1, Uppsala, Thursday, 6 October 2016 at 10:15 for the degree of Doctor of Philosophy. The examination will be conducted in English. Faculty examiner: Docent Gunnar Öhrwall (MAX IV Laboratory, Lund University).

Abstract

Oscarsson, J. 2016. Towards Mixed Molecular Layers for Dye-Sensitized Solar Cells. *A Photoelectron Spectroscopy Study*. *Digital Comprehensive Summaries of Uppsala Dissertations from the Faculty of Science and Technology* 1409. 81 pp. Uppsala: Acta Universitatis Upsaliensis. ISBN 978-91-554-9664-7.

The increasing demand for renewable energy has led to substantial research on different solar cell technologies. The dye-sensitized solar cell (DSC) is a technology utilizing dye molecules for light absorption. Dye molecules are adsorbed to a mesoporous semiconductor surface and after light absorption in the dye, charge separation occurs at this interface. Traditionally, DSCs have used layers of single dye species, but in recent efforts to enhance power conversion efficiency, more complex molecular layers have been designed to increase the light absorption. For example, the most efficient DSCs use a combination of two dye molecules, and such dye co-adsorption is studied in this thesis.

A key to highly efficient DSCs is to understand the dye/semiconductor interface from a molecular perspective. One way of gaining this understanding is by using an element specific, surface sensitive technique, such as photoelectron spectroscopy (PES).

In this thesis, PES is used to understand new complex dye/semiconductor interfaces. Dyes adsorbed to semiconductor surfaces are analyzed using PES in terms of geometric and electronic surface structure. The investigations ultimately target the effects of co-adsorbing dyes with other dyes or co-adsorbents.

PES shows that Ru dyes can adsorb in mixed configurations to TiO_2. Co-adsorption with an organic dye affects the configuration of the Ru dyes. As a consequence, shifts in energy level alignment and increased dye coverage are observed. The dyes are affected at a molecular level in ways beneficial for solar cell performance. This is called collaborative sensitization and is also observed in todays most efficient DSC.

Dye molecules are generally sensitive to high temperatures and the substantial decrease in power conversion efficiency after heat-treatment can be understood using PES. Furthermore, comparing two mesoscopic TiO_2 morphologies used in DSCs show differences in trap state density in the band gap, explaining the photovoltage difference in DSCs comprising these morphologies. Using mixed molecular layers on NiO results in significant improvements of p-type DSC power conversion efficiency. PES shows that changed adsorption configuration contribute to this effect.

This thesis shows that PES studies can be used to obtain insight into functional properties of complex DSC interfaces at a molecular level.

Keywords: dye-sensitized solar cell, DSC, mesoscopic solar cell, photoelectron spectroscopy, PES, XPS, interface, TiO2, NiO, co-adsorption, co-adsorbent, collaborative sensitization, mixed molecular layers

Johan Oscarsson, Department of Physics and Astronomy, Molecular and condensed matter physics, Box 516, Uppsala University, SE-751 20 Uppsala, Sweden.

ISSN 1651-6214
ISBN 978-91-554-9664-7
urn:nbn:se:uu:diva-301164 (http://urn.kb.se/resolve?urn=urn:nbn:se:uu:diva-301164)

To Elin, Sixten and Malte

List of papers

This thesis is based on the following papers, which are referred to in the text by their Roman numerals.

I **Geometrical and Energetical Structural Changes in Organic Dyes for Dye-Sensitized Solar Cells probed using Photoelectron Spectroscopy and DFT**
Susanna K. Eriksson, Ida Josefsson, Hanna Ellis, Anna Amat, Mariachiara Pastore, Johan Oscarsson, Rebecka Lindblad, Anna I. K. Eriksson, Erik M. J. Johansson, Gerrit Boschloo, Anders Hagfeldt, Simona Fantacci, Michael Odelius and Håkan Rensmo
Physical Chemistry Chemical Physics **18**, 252-260, 2016

II **Molecular Degradation of D35 and K77 Sensitizers when Exposed to Temperatures Exceeding 100 °C Investigated by Photoelectron Spectroscopy**
Johan Oscarsson, Kristofer Fredin, Sareh Ahmadi, Anna I. K. Eriksson, Erik M. J. Johansson and Håkan Rensmo
Physical Chemistry Chemical Physics **18**, 8598-8607, 2016

III **Coadsorption of Dye Molecules at TiO_2 Surfaces: A Photoelectron Spectroscopy Study**
Johan Oscarsson, Maria Hahlin, Erik M. J. Johansson, Susanna K. Eriksson, Rebecka Lindblad, Anna I. K. Eriksson, Azhar Zia, Hans Siegbahn and Håkan Rensmo
The Journal of Physical Chemistry C **120**, 12484-12494 , 2016

IV **Interface Structure Effects upon Co-Adsorption of Black Dye and D35 on TiO_2**
Johan Oscarsson, Susanna K. Eriksson, Rebecka Lindblad, Erik M. J. Johansson, Anna I. K. Eriksson, Hans Siegbahn and Håkan Rensmo
In manuscript

V **Mesoporous TiO_2 Microbead Electrodes for Solid State Dye-Sensitized Solar Cells**
Meysam Pazoki, Johan Oscarsson, Lei Yang, Byung-Wook Park, Erik M. J. Johansson, Håkan Rensmo, Anders Hagfeldt and Gerrit Boschloo
RSC Advances **4**, 50295-50300, 2014

VI **Enhancement of p-Type Dye-Sensitized Solar Cell Performance by Supramolecular Assembly of Electron Donor and Acceptor**
Haining Tian, Johan Oscarsson, Erik Gabrielsson, Susanna K. Eriksson, Rebecka Lindblad, Bo Xu, Yan Hao, Gerrit Boschloo, Erik M. J. Johansson, James M. Gardner, Anders Hagfeldt, Håkan Rensmo and Licheng Sun
Scientific Reports **4**, 4282, 2014

Reprints were made with permission from the publishers.

Extended bibliography

The following papers that I have co-authored are not included in the thesis:

Dipicolinic Acid: A Strong Anchoring Group with Tunable Redox and Spectral Behavior for Stable Dye-Sensitized Solar Cells
Erik Gabrielsson, Haining Tian, Susanna K. Eriksson, Jiajia Gao, Hong Chen, Fusheng Li, Johan Oscarsson, Junliang Sun, Håkan Rensmo, Lars Kloo, Anders Hagfeldt and Licheng Sun
Chemical Communications **51**, 3858-3861, 2015

Chemical and Electronic Structure Characterization of Lead Halide Perovskites and Stability Behavior under Different Exposures - A Photoelectron Spectroscopy Investigation
Bertrand Philippe, Byung-Wook Park, Rebecka Lindblad, Johan Oscarsson, Sareh Ahmadi, Erik M. J. Johansson and Håkan Rensmo
Chemistry of Materials **27**, 1720-1731, 2015

Electronic Structure of $CH_3NH_3PbX_3$ Perovskites: Dependence on the Halide Moiety
Rebecka Lindblad, Naresh K. Jena, Bertrand Philippe, Johan Oscarsson, Dongqin Bi, Andreas Lindblad, Suman Mandal, Banabir Pal, D. D. Sarma, Olof Karis, Hans Siegbahn, Erik M. J. Johansson, Michael Odelius and Håkan Rensmo
The Journal of Physical Chemistry C **119**, 1818-1825, 2015

Electronic Structure of TiO_2/$CH_3NH_3PbI_3$ Perovskite Solar Cell Interfaces
Rebecka Lindblad, Dongqin Bi, Byung-Wook Park, Johan Oscarsson, Mihaela Gorgoi, Hans Siegbahn, Michael Odelius, Erik M. J. Johansson, and Håkan Rensmo
The Journal of Physical Chemistry Letters **4**, 648-653, 2014

Comments on my own contribution

The results presented in this thesis are a product of close collaborations between people with different expertise and my position in the author list reflects my contribution well. My responsibility was generally the photoelectron spectroscopy (PES) measurements and their interpretation, while characterization of solar cells and theoretical calculations were performed by others.

In Paper I, I participated in the PES measurements and analysis and had the main responsibility for the submission and revision process of the manuscript. In Paper II, I performed the PES measurements and analysis and had the main responsibility of writing the manuscript. In Paper III, I performed parts of the PES measurements and analysis and had the main responsibility for writing the manuscript. In Paper IV, I contributed to planning and performing the PES measurements, I was responsible for the data analysis and wrote the manuscript. In Paper V, I was responsible for the PES measurements and analysis and wrote parts of the manuscript. In Paper VI, I planned and performed the PES measurements and data analysis as well as wrote parts of the manuscript.

Contents

1. Introduction

1.1 Global energy production

The use of energy steadily increases globally and fossil fuels are dominating the energy production which leads to an increased emission of greenhouse gases (mostly CO_2). The worldwide stock of fossil fuels steadily decreases, so there is a large demand to increase the production of renewable energy. There are a number of sources of renewable energy as: hydro, wind, bio, solar and geothermal power. Globally, 24 % of the electricity production came from renewable energy sources in the end of 2015 [1]. Hydropower has the largest share of the renewable electricity production, followed by wind, bio, solar and geothermal power.

A solar cell, or a photovoltaic (PV) device, can convert solar irradiation into electricity. The energy emitted by the sun reaching Earth is about $1.7 \text{x} 10^5$ TW out of which around 600 TW is estimated to be available for use, when accounting for reflections and the land area of the Earth [2]. The global energy consumption is around 15 TW as a comparison. Thus, the possibilities for renewable energy production by means of PV devices are great. A rough calculation reveals that if 0.1 % of the surface of the Earth was covered with solar cells having a 10 % power conversion efficiency, the global energy needs would be fulfilled [3].

In Sweden, the situation is very different from the average numbers presented above. Hydropower and nuclear power stand for over 40 % of the electricity production each and wind power 7 % [4]. Thus, the emission of CO_2 from the production of electricity is much lower in Sweden compared to the global average. Solar power has only 0.06 % of the total electricity production [4, 5]. However, 36 MW of solar power was installed in 2014 meaning that for the fourth consecutive year, the solar cell market in Sweden doubled in size [5].

The numbers given above focus on the production of electricity. The transport sector is a large consumer of energy, predominantly from fossil fuels. The interest for electrically powered vehicles is growing and with that comes the demand for even more renewable energy to charge the batteries of the vehicles.

1.2 Solar cells

As already mentioned, the sun provides enormous amounts of energy for the Earth and a sustainable way to harvest part of that energy is through the use of

solar cells. A solar cell is a device capable of directly converting sunlight into electricity by means of light absorption and charge separation. After manufacturing, the only thing needed for production of electricity is sunlight, which leaves no rest products behind. The first report of a solar cell with decent power conversion efficiency came in 1954 and it was achieved in a silicon based cell [6]. Since then, a lot of research has been done on different semiconductor materials, such as Si, GaAs, CdTe, CIGS (Copper Indium Gallium Selenide) and CZTS (Copper Zinc Tin Sulfide). Silicon can give solar cells with a power conversion efficiency around 25 %, but they are expensive to produce, whereas the others are not as efficient and cheaper to produce. However, some of the constituents of the above mentioned semiconductors exist in very limited amounts on Earth, so there is an interest in other solar cell technologies not using them.

During the last 25 years, alternative techniques have emerged to take up the competition. Some competitors are based on organic molecules or dye molecules. These new technologies have lower production costs than the crystalline semiconductors and they are generally made from abundant materials. One of these technologies is the dye-sensitized solar cell (DSC) which has gained a lot of research interest since 1991, when the first breakthrough was reported [7]. The photoactive component in a DSC is a mesoporous semiconductor electrode which is sensitized by dye molecules for light absorption. This thesis concerns the understanding of DSC interfaces and the DSC will be described in more detail in Chapter 2.

The power conversion efficiency of a solar cell depends on its ability to absorb incoming photons, i.e. it depends on the overlap between the absorption spectrum of the solar cell and the spectrum of the light source. For outdoor use, the light source is the sun and therefore it is important to find absorbers that efficiently overlap with the solar spectrum. The semiconductor materials mentioned above have a high light absorption in the red part of the visible spectrum, where a large part of the outdoor solar spectrum is also found. However, indoor applications may also be an important area for use of solar cells in the future. For indoor use, the most common light source is fluorescent lamps, having a significant part of the spectrum at shorter wavelengths, where e.g. Si absorbs poorly. DSCs have a tuneable (by choice of dye) spectral response making them a good candidate for indoor applications. Moreover, the average indoor lighting levels are 2-3 orders of magnitude lower than outdoor conditions. Studies have shown that DSCs outperform other kinds of solar cells in indoor conditions [8]. Furthermore, DSCs are cheap to produce compared to other kinds of solar cells and they can be prepared on flexible substrates in various shapes. This makes them ideal for integration in consumer products for indoor use, e.g. chargers for electric devices like smart phones, tablets and laptops.

The most efficient DSCs of today comprise a mixture of two dyes on a TiO_2 surface as the photoactive part of the solar cell [9]. To increase the power

conversion efficiency of the cell, the dyes have been chosen to have complementary light absorption properties, i.e. their absorption spectra are shifted in wavelength relative to each other. Such a complex system could produce high efficiency solar cells, but the knowledge on how multiple dyes (or dyes with co-adsorbents) affect each other from a molecular point of view (in terms of dye coverage, adsorption configuration and energy level alignment) is limited. These parameters are of great importance for the function of the DSC, and investigations of them are beneficial for the future development of highly efficient DSCs.

1.3 This thesis

To be able to produce DSCs with high power conversion efficiencies, detailed knowledge of the components in the cell is a necessity. The photoactive part of a DSC is a semiconductor film with dye molecules adsorbed to it. Charge separation is realized at this interface. It is therefore crucial to understand the properties, e.g. dye coverage, adsorption configuration of the dye molecules and energy level alignment between dye and semiconductor, of the interface. To be able to gain this understanding experimentally, an element specific technique capable of detecting small chemical changes at material interfaces is beneficial. In this thesis, photoelectron spectroscopy (PES) (described in Chapter 3.1) has been used as a tool with these capabilities. The goal with the work presented here has been to explore how this technique can be used to increase the understanding of complex interfaces between dye and mesoscopic oxides recently developed for use in efficient DSCs.

Thin mesoporous semiconductor films sensitized with one dye have been investigated by means of PES for quite some time and there is a large amount of information available. Lately, the most efficient DSCs use multiple dyes co-adsorbed to the semiconductor. Interfaces of this kind are not as well studied, but they are highly interesting due to the power conversion efficiency of the DSCs. By increasing the number of dyes also the complexity of the system increases. In this thesis, PES has been used to get a fundamental understanding of what happens when multiple dyes are used as well as when co-adsorbents are present in the molecular layer.

This thesis contains studies using TiO_2 as semiconductor substrate, both in its most common mesoscopic morphology for DSCs as well as a morphology that has shown great promise for the use in solid state DSCs, as well as studies using NiO as a substrate. Dye molecules with small differences in chemical structures are studied to deduce the effect of the subtle changes in structure. The thesis also contains studies of dye molecules subjected to elevated temperatures, which is important to have knowledge of both during manufacturing and in operation. Furthermore, there are studies of mixed molecular layers (dye/dye and dye/co-adsorbent), both on TiO_2 and NiO included in the thesis.

In the mixed dye/dye samples, the dye molecules affect each other at a molecular level in ways that are beneficial for the function of the DSC. This kind of interaction is known as a collaborative sensitization process.

1.3.1 Outline of the thesis

Chapter 2 describes the dye-sensitized solar cell and the parts it is made from. In Chapter 3, the main technique used, photoelectron spectroscopy, is introduced together with some basic solar cell characterization tools and sample preparations. Chapter 4 summarizes the results obtained and Chapter 5 gives an outlook towards the future. The thesis is then concluded with a popular scientific summary in Swedish in Chapter 6 and acknowledgements in Chapter 7.

2. Dye-sensitized solar cells

Dye-sensitized solar cells (DSCs) are based on a simple general structure. They have a working electrode consisting of conducting glass (usually FTO or ITO) covered by a mesoporous semiconductor film sensitized by dye molecules for light absorption. The mesoporous structure enhances the surface area approximately by a factor 1000 (for a 10 μm thick film) [7, 10], enabling higher dye loading and consequently, higher light absorption. The semiconductor can be n-type or p-type and the basics of both will be described in this chapter. In contact with the working electrode is a hole transporting material, which can be a liquid electrolyte with a redox mediator or a solid state hole conductor. DSCs also have a counter electrode, which in liquid DSCs consist of conducting glass covered with a catalyst, most commonly platinum or carbon based. For solid state devices, the counter electrode is a thin layer of metal evaporated onto the hole conductor.

The story of the DSC started with low efficiency solar cells based on flat semiconductor surfaces and during the 1970s-1980s the first papers heading towards the DSC we know today were published [11–13]. The paper of O'Regan and Grätzel in 1991 [7] was the first report utilizing a mesoporous semiconductor substrate with a power conversion efficiency of 7-8 %. From this point the evolution in the DSC field lifted off and since then, a lot of work has been carried out in the field [10, 14–16] and the highest power conversion efficiencies today reach 12 %, using a single dye as sensitizer [17, 18]. Co-adsorbing several dyes with complementary light absorption properties to the semiconductor structure has been tried for quite some time, without real success [10]. Lately, with the implementation of new dye structures and redox couples, as will be discussed later, the power conversion efficiency has been improved [19–22]. The highest power conversion efficiency of a DSC today is 14 % [9], which is obtained in a system comprising two dyes. During the last few years, perovskite materials and quantum dots have successfully been implemented as light absorbers. Power conversion efficiencies exceeding 22 % are realized using perovskites, whereas quantum dots give around 11 % [23]. This thesis focuses mainly on traditional DSCs.

2.1 Materials

This section will give an introduction to the main components of a DSC as mentioned above; the semiconductor, the dye and lastly the electrolyte and its redox active components.

2.1.1 The semiconductor

The electrons in an atom are represented by their orbital structure. Different elements have a unique distribution of electrons, and when atoms are brought together their orbitals will overlap and interact with each other. If the orbital overlap is large and the orbital energies are similar, the interaction is strong. As a consequence of this, new molecular orbitals (MOs) with different energies will be formed. Increasing the size of the molecule (bringing more atoms together) leads to an increase in the complexity and consequently the number of MOs. A higher number of MOs means that the separation in energy between the MOs will be lower.

When going to solid crystals, e.g. semiconductors, metals or insulators, they can be regarded as very large molecules with periodic structure of interacting orbitals. In this picture, the number of MOs will be enormous and they will be so closely spaced in energy that they form energy bands that are characterized by the density of states (DOS), i.e. the number of available states per unit energy. This is true both for occupied and unoccupied states and the bands are referred to as the valence (VB) and conduction bands (CB) respectively, as schematically illustrated in Figure 2.1. In the case of metals, the top band would be partially filled with electrons. The energy at which the highest occupied electronic state is found is referred to as the Fermi level (E_F), which can also be called the electrochemical potential (μ). For semiconductors and insulators on the other hand, the VB and CB are separated by a gap in energy, the band gap (E_g). The difference between a semiconductor and an insulator is the size of the band gap, where in semiconductors thermal excitations of electrons from VB to CB is possible, while they are much less probable in insulators.

The conductivity of a semiconductor is dependent on the concentration of charge carriers (electrons in CB and holes in VB). In the ground state at 0 K, the VB is filled and the CB is empty, meaning that no charge carriers exist. In order to have conductivity, excitations of charge carriers are necessary. The concentration of charge carriers is given by the Fermi-Dirac distribution [24, 25]. From the distribution, the Fermi level is defined as the energy where the probability of finding an occupied energy level is exactly one half. In the case of an undoped (intrinsic) semiconductor, the Fermi level is found in the middle of the band gap (at 0 K), as shown in Figure 2.1(a). The energy at which an electron is regarded to have left the material is called the vacuum level (E_{vac}). The energy difference between the vacuum level and the Fermi level is known as the work function of the material (ϕ), as shown in Figure 2.1 and discussed in Chapter 3.1.1.

Adding defects or impurities to the semiconductor lattice will break the periodicity of the crystal and thereby perturb the energy levels, which might have vast consequences on the properties of the semiconductor. If doing this in a controlled way it is called doping. Adding extra occupied energy levels close

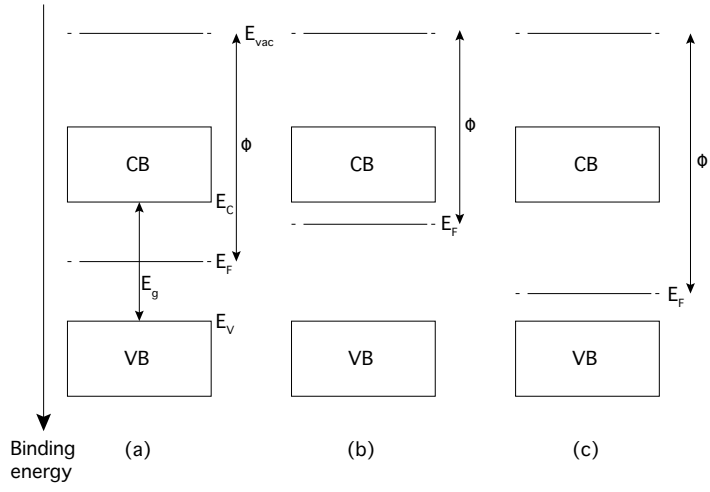

Figure 2.1. Schematic illustration of the band structure in semiconductors. CB is the conduction band (with the edge at E_C) and VB is the valence band (with the edge at E_V) separated by the band gap (E_g). E_F is the Fermi level, E_{vac} is the vacuum level and ϕ is the work function, i.e. the energy difference between them. (a) shows an ideal undoped semiconductor while (b) and (c) show n-doped and p-doped semiconductors respectively.

to the conduction band edge leads to donations of electrons to the CB. This is known as n-doping (giving an n-type semiconductor) and causes the Fermi level to shift closer to the CB edge, as shown in Figure 2.1(b). Consequently, extra unoccupied energy levels close to the valence band edge will accept electrons from the VB increasing the density of holes in the VB. This shifts the Fermi level closer to the VB edge and is known as p-doping (giving p-type semiconductors), as shown in Figure 2.1(c).

The by far most used semiconductor in n-type DSCs is TiO_2, but others like ZnO, SnO_2 and Nb_2O_5 as well as various semiconductor core-shell structures have also been used [3, 10, 26–30]. For p-type DSCs, most of the work is carried out using NiO as semiconductor substrate. In the work presented in this thesis, the n-type semiconductor TiO_2 has been used in Paper I-V and the p-type NiO in Paper VI.

TiO_2 is one of the most studied oxide semiconductors, mostly since it is very stable in a variety of conditions. The most common crystal structures are rutile and anatase and the TiO_2 pastes used to prepare TiO_2 electrodes for the work presented here consist of anatase nanoparticles. Anatase TiO_2 has a band gap of 3.2 eV and the Ti atoms in TiO_2 are found in a Ti^{4+} state, leaving the 3d orbital empty. Therefore, the conduction band of TiO_2 has predominantly a Ti3d character and the valence band O2p character [31]. TiO_2 is an n-type semiconductor since a deficiency in oxygen leaves an excess of electrons in the CB.

NiO is the most commonly used p-type semiconductor for DSCs and has also been studied for a long time due to its stability and versatility [32]. Ni in its atomic ground state has a $4s^2 3d^8$ electronic configuration. In NiO, Ni atoms are found in a Ni^{2+} state. An excess of oxygen however causes some of the Ni^{2+} to oxidize into Ni^{3+}, leaving behind empty electronic states close to the valence band edge [33–35], leading to it being a p-type semiconductor. The VB of NiO consist predominantly of a hybrydization of Ni3d and O2p, whereas the CB is dominated by Ni3d character [36–38]. NiO has a band gap of around 3.5-4.0 eV, making it a good candidate for use in p-type DSCs as well as substrate for catalysing solar fuel production.

2.1.2 The dye

There are many kinds of dye molecules used for DSCs [10]. They can be grouped into families from their chemical structures. Even though the dye families can have very different structures, all kinds of dyes share some important parts and characteristics, i.e. anchoring group (for adsorption to the semiconductor surface) and energy levels that ideally should match the light source (in terms of the light absorption spectrum of the dye matching the emission spectrum of the light source) and the different materials used in the complete DSC. The most frequently used anchoring group is carboxylic acid (-COOH), but also other ones are used, e.g. phosphonic acid ($-PO(OH)_2$) [10]. All dyes and adsorbents presented in this thesis utilize carboxylic acid anchoring groups, except DPA, used in Paper III, which has a phosphonic acid anchoring group.

For a basic description of the function of a DSC, important energy levels of a dye molecule are the highest occupied molecular orbital (HOMO) and lowest unoccupied molecular orbital (LUMO), as discussed in Chapter 2.2. Spectroscopically, information on the HOMO level can be gained from e.g. PES and electrochemical measurements, whereas the LUMO can be studied by X-ray absorption (see Chapter 3.1.8). The energy difference between the HOMO and LUMO levels can be studied using UV-vis spectroscopy (see Chapter 3.2.1).

The work presented in this thesis is based on dye molecules from two frequently used, well studied dye families; organic triarylamine (TAA) based dyes and metal-organic dyes based on Ru. These families are described in the following sections.

2.1.2.1 Sensitization of the semiconductor surface

Adsorption is the process in which a species (adsorbate) binds to a surface (substrate). Typically one differs between physisorption and chemisorption, depending on which type of interaction is responsible for the adsorption. An adsorbate is physisorbed when it interacts with the substrate via electrostatic or van der Waals' forces and is thereby held in place. This is generally a weak

interaction between adsorbate and substrate. On the contrary, chemisorption is often a strong interaction through overlapping electronic orbitals from adsorbate and substrate, leading to the formation of a chemical bond. The interaction is of covalent or ionic type. More general details are found in various textbooks [39, 40]. In the context of this thesis, the process of adsorption refers to the binding, i.e. chemisorption, of dye molecules and co-adsorbents to TiO_2 or NiO electrodes. In order for a dye molecule or co-adsorbent to chemisorb to the semiconductor surface, an anchoring group is a necessity in the chemical structure. Upon such adsorption using carboxylic acid anchoring groups, the proton is removed from the anchoring group of the adsorbate, which instead binds to the metal atoms (Ti or Ni) in the semiconductor. A brief introduction to some commonly used adsorption models will be given below.

When adsorbing dye molecules from solution, the adsorption process is thermodynamically described as an equilibrium between free (solvated) and adsorbed species. When studying adsorption of different species, an adsorption isotherm is used to illustrate the adsorption behaviour. An adsorption isotherm is often represented as the surface concentration (coverage) of adsorbed species as a function of the concentration of free species (i.e. the bulk concentration in solution), at a given constant temperature. A mathematical model based on the shape of the isotherm can be used to characterize the adsorption mechanism of the studied species. There is a large number of models developed to cover all kinds of adsorption behaviour.

A model that is well-known and simple is the Langmuir model [24, 40–42]. This is an idealistic model that assumes that all adsorption sites of the substrate are equal, that no interaction takes place between adsorbates and that the maximum coverage possible is a monolayer. To account for more complex situations, e.g. interactions between adsorbates, models accounting for more than monolayer coverage need to be used [24, 41, 43–45].

Based on the discussion above, it is easy to understand that the formation of a dye-sensitized surface can be very complex depending on e.g. solubility, adsorption energy, adsorption sites and intermolecular interactions. When forming mixed molecular layers, the complexity increases even more. Paper I-IV address these structures, where Paper III and IV in particular highlight the effects of mixing.

2.1.2.2 Organic TAA dyes

There are today many different organic dye molecules from various dye families that provide highly efficient DSCs [10, 46–50]. In this thesis, organic dyes comprising a TAA unit have been used, as previously mentioned. The dye molecules D35 [51], D45 [52] and LEG4 [53, 54] (see Figure 4.1 in Chapter 4) are all based on TAA and stem from the well studied D5 dye [55]. These dyes have a donor- π linker- acceptor architecture (D-π-A), which is illustrated in Figure 2.2; schematically in (a) and illustrated on the D5 molecule

in (b). Adsorption to a semiconductor surface is done via the anchoring group, which consequently is a part of the acceptor unit.

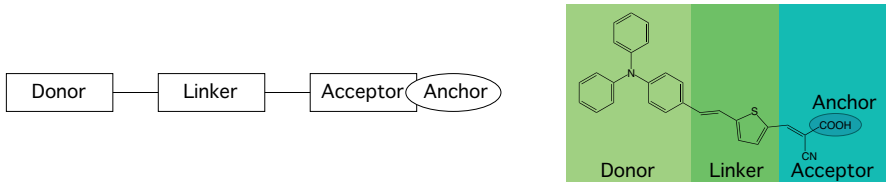

Figure 2.2. Schematic illustration of the donor - π linker - acceptor dye architecture for use in n-type DSCs in (a). The position of the anchoring group is on the acceptor unit and the overlap indicates that the anchoring group itself can be a part of the acceptor unit. (b) illustrates the architecture applied on the D5 dye.

The D-π-A dye architecture is used for distinguishing between different parts of the molecules. This separation facilitates easy modifications of the dye molecules by modifying one of the three parts, which allows for tuning of the properties of the dye. The HOMO level of these dye molecules is mainly located on the TAA part of the dyes with some contribution from the ligands attached to it [48, 51, 55–57]. Thus, the TAA with the ligands constitute the donor part of the molecules. The LUMO should be centered away from the HOMO, on the acceptor. In between the donor and acceptor parts, a π conjugated linker is found. The linker should facilitate charge transfer from HOMO to LUMO and inhibit charge recombination simultaneously. By changing the donor part of the molecule, the HOMO properties can be altered. The linker unit can be altered, e.g. in length, to tune the optical properties of the dye molecule [46, 48, 50, 55]. To modify the LUMO, changes can be done to the acceptor part.

2.1.2.3 Metal-organic Ru-based dyes

Ru-based dye molecules have been used as sensitizers for DSCs for a long time. Traditionally and still, Ru-based dyes give DSCs with high power conversion efficiencies [10, 46, 47, 58–62]. Traditionally, this dye family has a Ru center to which the ligands are coordinated. Usually the Ru center is connected to thiocyanate (NCS) and bipyridine/terpyridine ligands on which the anchoring groups and other ligands are situated. The Ru-based metal-organic dye molecules K77 [63], Z907 [64] and BD [59] are shown in Figure 4.2 in Chapter 4 together with the co-adsorbent DPA used with Z907 in Paper III. Most Ru-based dyes have the HOMO level predominantly located on the Ru atom with contributions from the NCS ligands, and it has a Ru4d character [65–67]. The LUMO of similar Ru-based dyes has previously been shown to be located on the bipyridine/terpyridine ligands [68, 69]. The HOMO and LUMO are schematically shown on the BD molecule in Figure 2.3. Excitation

of electrons from HOMO to LUMO is facilitated via metal to ligand charge transfer (MLCT). The carboxylic acid anchoring groups are situated on the bipyridine/terpyridine ligands, so when an electron is excited to the LUMO it is spatially close to the semiconductor surface facilitating fast electron injection into the CB of the semiconductor.

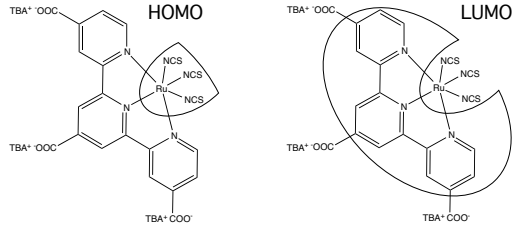

Figure 2.3. Schematic illustration of spatial HOMO and LUMO positions of a Ru-based dye with BD as an example. Figure adapted and modified from reference [70].

2.1.2.4 Dyes for p-type DSCs

In a p-type DSC, as schematically illustrated in Figure 2.6, photon absorption of the dye, often described by electron excitation from HOMO to LUMO of the dye, is followed by the injection of a hole from the dye into the VB of the semiconductor. The reduced dye molecule is then regenerated by electron transfer from the LUMO level of the dye to the redox couple. The chemical structure of a porphyrin based dye used in Paper VI is shown in Figure 4.3 in Chapter 4, together with a fullerene derivative used as a co-adsorbent. Since a p-type DSC operates "in reverse" to its n-type counterpart, the dye molecules used need to be designed differently. To facilitate hole injection into the semiconductor, the anchoring group of p-type dyes should be located on the donor part of the molecule, as schematically illustrated for a D-π-A dye for use in a p-type DSC in Figure 2.4.

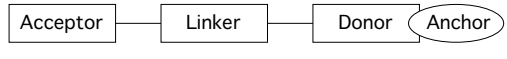

Figure 2.4. Schematic illustration of the donor - π linker - acceptor dye architecture for use in p-type DSCs. The position of the anchoring group is on the donor unit and the overlap indicates that the anchoring group itself can be a part of the donor unit.

2.1.2.5 The role of co-adsorbents in DSCs

Most co-adsorbents used in DSCs don't absorb any light, i.e. they will not directly contribute to the performance of the DSC. The co-adsorbent is added to modify the properties of the photoactive (dye) layer, thereby ultimately improving the power conversion efficiency of the DSC. The modifications can be e.g. to minimize dye-dye interactions on the surface, reduce dye aggregation, modifications of the energy level alignment in the DSC or passivation of trap states in the semiconductor.

2.1.3 The electrolyte

A majority of the papers this thesis is built upon deals with "traditional" DSCs, i.e. DSCs comprising liquid electrolytes. A solid state hole conductor works similarly as an electrolyte (information on the most commonly used hole conductor, spiro-OMeTAD can be found elsewhere [10, 71]). The discussion in this section will be based on liquid electrolytes.

A liquid electrolyte generally consists of a redox couple (together with additives) in a solvent. For the function of a DSC, the redox potential of the redox couple is the level of importance. It should be higher in energy than the accepting level of the dye in order to have a driving force for dye regeneration. At the same time, it should not be too high in energy since more voltage than necessary will be lost from the DSC output. The most used redox couple is iodide/triiodide (I^-/I_3^-), which was used in the DSC breakthrough paper by O'Regan and Grätzel in 1991 [7]. I^-/I_3^- has since then been successfully used in DSCs yielding high power conversion efficiencies [9, 10, 72]. The success of this redox couple has been ascribed to its slow recombination with electrons from TiO_2, which in turn probably depends on the fact that multiple electron transfers take place during each redox cycle [10, 73, 74]. There are also some disadvantages with I^-/I_3^-, the main ones being: the highly negative redox potential limiting the voltage output of the DSC, it is coloured making it compete with the dye for light absorption, and its highly corrosive nature, which is capable of corroding most metals [75–77]. These drawbacks of the I^-/I_3^- redox couple started the search for alternatives. A number of different redox couples have been tried [10], but one of the first really successful competitors to I^-/I_3^- were cobalt complex based redox couples in combination with a new dye design in 2010 and 2011 [17, 49]. The most efficient DSC as of today utilizes a cobalt complex based redox couple in combination with two co-adsorbed dyes [9].

2.2 Working principle and materials used in n-type DSCs

As mentioned earlier, a DSC has three main components: working electrode, counter electrode and a hole transporting material. In Figure 2.5, a schematic illustration of a DSC based on the n-type semiconductor TiO_2 is shown. The dye molecule is illustrated by two energy levels, D/D^+ and D^*/D^+. D/D^+ describes the potential for oxidation of the dye and is related to the highest occupied molecular orbital (HOMO) energy of the dye molecule. In the measurements presented in this thesis, the properties of the HOMO level will be addressed by PES. In a PES measurement, electrons are emitted quickly from the sample. Thus, the bonds in the molecule will not have time to relax before the electron leaves. On the contrary, electrochemical measurements are

performed in solution, where relaxation of the bonds occur during the measurement. The experimentally obtained values can be compared to theoretical density functional theory (DFT) calculations. In a similar way, D^*/D^+ is related to the lowest unoccupied molecular orbital (LUMO) of the dye.

The arrows in Figure 2.5 indicate electron transfer reactions and the numbers given in the figure are used in the text. When a DSC is illuminated, a photon is absorbed and an electron in the dye molecule is excited from from the ground state (D) to an excited state (D^*) of the dye molecule, process (1) in the figure. The energy needed for this excitation should be in the visible light regime. After excitation, the electron is injected into the conduction band (CB) of the semiconductor, leaving the dye in an oxidized state (D^+) (2). The dye molecule is thereafter reduced by the redox mediator (E_{redox}) (3). Electrons injected into TiO_2 diffuse through the mesoporous structure to the back contact, where they are collected and transferred to an external circuit to perform electrical work. After that, the electrons are returned to the redox mediator via the counter electrode and the redox couple is reduced.

There are also back-electron transfer reactions that should be avoided. The main ones are: relaxation within the dye molecule (4), recombination of the injected electron to the dye molecule (5) and recombination to the redox mediator (6).

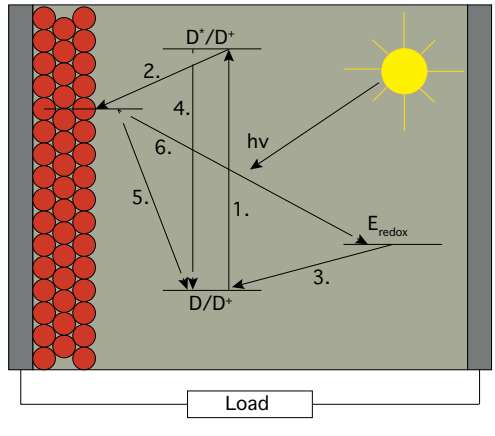

Figure 2.5. Schematic illustration of an n-type DSC. Solid arrows mark the electron transfer under illumination, whereas the dashed arrows indicate back-electron transfer limiting the overall performance of the cell.

The function of a DSC is heavily dependent on the kinetics in the system and the time scales at which electron transfer occur are of great importance. The time scales associated with the electron transfer reactions are [10, 78, 79]:

(2) fs - ps
(3) μs
(4) ns
(5) μs - ms

(6) μs

while photon absorption and subsequent electron excitation (1) is regarded to be instantaneous.

In order to drive electrons in the desired direction in the DSC, some driving force is necessary. The potential difference between D^*/D^+ of the dye and the conduction band edge of the semiconductor gives a driving force that determines the rate of electron injection into the TiO_2, whereas the potential difference between the redox potential of the redox mediator and D/D^+ of the dye gives a driving force for the rate of regeneration of the dye. The maximal theoretical photovoltage a DSC can provide is set by the potential difference between the Fermi level of electrons in the TiO_2 and the redox potential of the redox mediator at the counter electrode during operation. This is in reality lowered by resistance in the cell. The photocurrent is limited by the light harvesting efficiency, the injection efficiency, the regeneration efficiency and the charge collection efficiency, as seen in Equation 3.10.

Some factors influencing the above and thus affecting the photovoltage and photocurrent from the DSC are the coverage of the dye molecules on the semiconductor surface, the stoichiometry of the adsorbed dye molecules, the energy level alignment between the components of the DSC and the electronic structure of the dye molecules. All these factors have been studied and will be presented in this thesis.

2.3 Working principle and materials used in p-type DSCs

The power conversion efficiency of p-type DSCs is in general lower than for the n-type counterpart. There is however a large research interest in the field of p-type DSCs. The main interest is driven by the possibility to make tandem solar cells, consisting of a p-type and an n-type device sandwiched together to form a solar cell. This concept is interesting due to the possibility to increase the light harvesting efficiency (LHE), i.e. the absorption of a larger part of the solar spectrum at a higher efficiency, by an appropriate choice of components. The components in this case mostly refer to choosing dyes for the n- and p-type cells that have complementary light absorption properties as well as the electrolyte composition, but also choosing the semiconductors wisely. When stacking two devices together, the photovoltage from both is additive, but the photocurrent is limited by the device with the lowest photocurrent, which so far has been the p-type device. The maximum theoretical power conversion efficiency is described by the Shockley-Queisser limit [80]. For a single junction, the maximum is 31 %, whereas for a double junction device, as a tandem cell, it is 42.5 % [80–83]. Therefore, extensive research is ongoing to increase the photocurrent and power conversion efficiency of p-type DSCs.

The most used semiconductor in p-type DSCs is NiO, which is transparent and very stable in a broad variety of conditions. A schematic illustration of a p-type DSC under illumination is shown in Figure 2.6. The numbers on the arrows in the figure are used in the text. The basic components are the same as for n-type DSCs and the working principle is as follows: electron excitation from HOMO to LUMO of the dye upon illumination (1). This is followed by hole injection from the dye into the valence band of the NiO (2) and electron transfer from the LUMO of the dye to the redox mediator (3). The back reactions limiting the efficiency of the DSC are: electron recombination within the excited dye molecule (4), recombination from the LUMO of the dye to the valence band of the semiconductor (5) and recombination from the redox mediator to the valence band of the semiconductor (6).

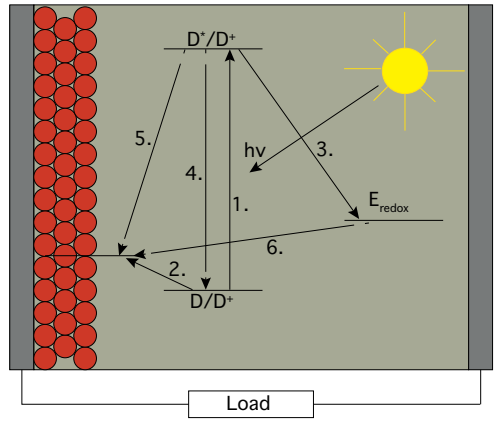

Figure 2.6. Schematic illustration of a p-type DSC. Arrows mark the electron and hole transfer under illumination. Solid arrows are desired charge transfer reactions, whereas the dashed ones are recombinations limiting the efficiency of the DSC.

3. Methods

In this chapter, the methods used in this thesis will be described. The focus will be on photoelectron spectroscopy (PES) and the experimental setups used. After the PES part, the main methods of solar cell characterization will be introduced followed by a description of sample preparations.

3.1 Photoelectron spectroscopy, PES

The following sections will provide a short introduction to photoelectron spectroscopy (PES). For a deeper description of the processes, information can be found in more comprehensive textbooks [84–87].

3.1.1 Basic principles

Photoelectron spectroscopy (PES) is a surface sensitive and element specific technique used for characterizing surfaces and interfaces of materials. The technique relies on the photoelectric effect, which was experimentally observed for the first time in 1887 by Heinrich Rudolf Hertz [88]. The photoelectric effect was explained by Albert Einstein in 1905 [89], awarding him the Nobel Prize in physics in 1921, and describes how electrons are emitted from a material when illuminated by photons having an energy exceeding a threshold value. Illuminating the sample with photons with a well defined energy, hν, results in emission of an electron if the incident photon energy is higher than the binding energy, E_B, of the electron in the sample. Conservation of energy gives:

$$E_K = h\nu - E_B \tag{3.1}$$

where E_K is the kinetic energy of the emitted photoelectron.

When working with metallic substrates, the Fermi level is often used as a point of energy reference. In this case a fourth term is added to equation 3.1. The added term (ϕ), is known as the work function of the sample and is defined as the difference in energy between the Fermi level and the vacuum level. The relation in this case is given by:

$$E_K = h\nu - E_B - \phi \tag{3.2}$$

Thus, by knowing the photon energy and measuring the kinetic energy of emitted photoelectrons, the binding energy of the electrons in the sample can be easily computed. The technique, also known as Electron Spectroscopy for Chemical Analysis (ESCA) or X-ray Photoelectron Spectroscopy (XPS), was developed by Kai Siegbahn and co-workers [90]. In 1981, Siegbahn was awarded the Nobel Prize in physics for his contribution to the development of PES [91].

To obtain a photoelectron spectrum, the number of emitted photoelectrons are measured as a function of the kinetic energy for a given photon energy. PES is generally divided into core level and valence level PES, depending on the origin of the photoelectron, as schematically illustrated in Figure 3.1. Core levels refer to localized levels with atomic character, usually at higher binding energies, while valence levels have a delocalized molecular character and are found at lower binding energies. Figure 3.2 shows examples of core level and valence level PES of a TiO_2 electrode sensitized with the organic dye D35.

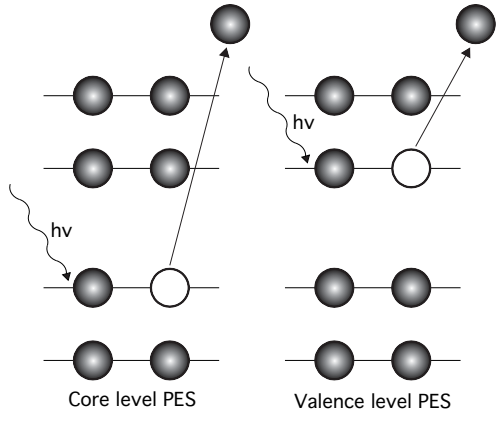

Figure 3.1. Schematic illustration of core level and valence level PES.

3.1.2 Binding energy and chemical shifts

The binding energy of an electron in an orbital depends on the difference in energy between the initial and final states. The initial state is the neutral system whereas the final state is the core-ionized system. This can be described by

$$E_B = E_{tot}(N-1) - E_{tot}(N) \tag{3.3}$$

where E_{tot} is the total energy of the initial state with N electrons and of the final state with $N-1$ electrons. To be able to calculate binding energies, different approximations have to be used. A simple way of calculating binding energies is by applying Koopmans' theorem, which assumes that no rearrangement of the remaining $N-1$ electrons takes place upon ionization. The binding energy

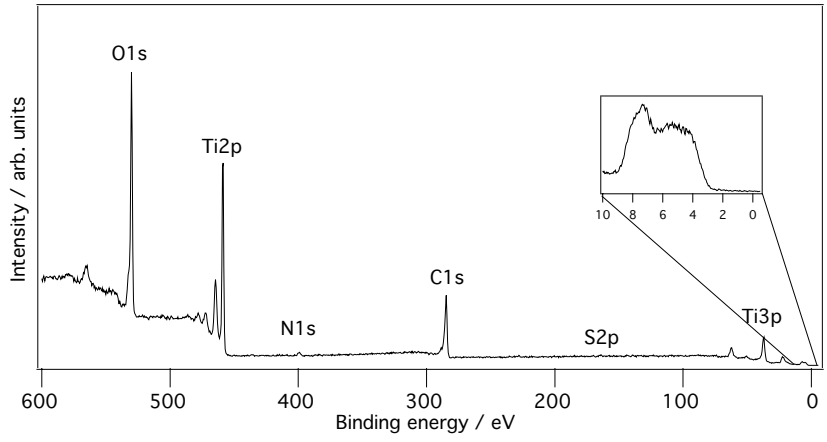

Figure 3.2. Overview PES spectrum of D35 on TiO_2 with a zoom in of the valence region in inset. The spectrum was measured using a photon energy of 758 eV.

is within this approximation found by solving the Schrödinger equation using Hartree-Fock wave functions for the N electron system [84]. Koopmans' theorem thus implies that the binding energies are given by the negative of the Hartree-Fock orbital energies [84]. However, in photoemission one electron is lost in the final state which means that the nucleus will not be as efficiently screened for the remaining electrons. This induces relaxations to the remaining electron orbitals, leading to relaxation energy corrections to the Koopmans' theorem binding energies. To include these corrections, more elaborate calculations performed on both the initial and final states need to be be done to obtain the total energy difference (see Equation 3.3). Calculations of this kind are often performed using density functional theory (DFT). A foundation of DFT is that a given electron density in a system corresponds to one single energy. The lowest energy configuration gives a density of states (DOS) that can be extracted for each constituting element (partial density of states, PDOS), which can be used to simulate PES spectra from which binding energies can be obtained.

Electrons originating from a certain core orbital have a characterstic binding energy, which however is affected by the chemical surrounding of the atom. This gives rise to what is known as chemical shifts [90]. The chemical shift contains both initial and final state effects [91], as expressed by Equation 3.3. One way to estimate the chemical shift is to use the $Z+1$ approximation, which means that the removal of a core level electron can be approximated by adding an extra charge unit to the nucleus, i.e. going from a nucleus with charge Z to one with charge $Z+1$ [84].

The chemical shift can also be roughly estimated by considering differences in electronegativity. Binding of the core ionized atom to an atom with a high electronegativity gives a higher binding energy than binding to an atom with

lower electronegativity. A very clear and famous example of this is comparing C-F to C-C, where the C1s signal is found at a higher binding energy when bound to fluorine (which has a high electronegativity) [90, 92].

3.1.3 Peak intensity

In a photoemission experiment, there are several parameters affecting the intensity, I, of a photoemission peak from an element situated at a depth d below the sample surface, as expressed by [87]:

$$I \propto F \frac{d\sigma}{d\Omega} \rho T e^{-\frac{d}{\lambda sin\theta}} \tag{3.4}$$

where F is the incident photon flux, $\frac{d\sigma}{d\Omega}$ is the differential photoemission cross section for the core level, ρ is the number density of the photoionized element at a depth d below the sample surface, T is the analyzer transmission of electrons, λ is the inelastic mean free path (IMFP) of electrons and $\frac{d}{sin\theta}$ thus is the distance the emitted photoelectron travels in the sample before leaving it, where θ is the angle between the sample surface and the direction of the spectrometer [87]. The photoemission cross section is specific for each atomic orbital and photon energy, generally it decreases with increasing photon energy. The IMFP is a measure of the distance a photoelectron can travel in a solid before losing energy due to inelastic collisions. The IMFP is dependent on the photoelectron's kinetic energy. The exponential term describes the attenuation of the PES signal as the emitted photoelectron travels within the sample before leaving it to enter the vacuum. This term describes the surface sensitivity of the technique, since photoelectrons originating deeper within the sample will be more affected by attenuation than electrons originating from the surface.

3.1.4 Hemispherical analyzers

A hemispherical analyzer is the most common type of electron energy analyzer. It consists of two concentric hemispheres separated by a certain distance. An electrostatic field is applied between the two hemispheres. Electrons emitted from the sample are transferred by a lens system to the analyzer entrance and accelerated or retarded to the analyzer pass energy. The electrons enter the analyzer via an entrance slit and the electrostatic field in the analyzer forces them to take a curved trajectory towards the detector. Depending on the kinetic energy of the electrons they will take different trajectories leading to them ending up on different positions of the detector. The detector consists of MCPs (micro-channel plates) followed by a fluorescent screen and a CCD camera that detects and counts the electrons hitting the fluorescent screen. The spectrometer is usually run in what is known as swept mode. This means that the voltages of the focusing optics (lens system) are scanned over the kinetic

energy range of interest. A consequence of this mode of operation is that every energy within the energy range has passed all positions of the detector. This gives in general more reliable spectra since possible irregularities of the detector are evened out. The analyzer can also be operated in fixed mode meaning that the voltages are not scanned and all electrons of a given kinetic energy will be detected at the same position of the detector. To obtain a photoemission spectrum, the electron counts are integrated over a certain time (dwell time). This is plotted versus the kinetic or binding energy of the electrons. A schematic drawing of a Scienta R4000 hemispherical analyzer is shown in Figure 3.3.

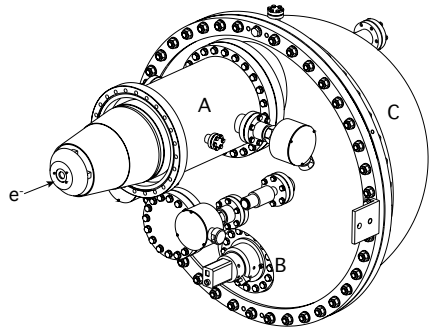

Figure 3.3. Schematic drawing of a Scienta R4000 analyzer. A indicates the lens system, where the arrow shows where electrons enter, B is the detector and C is the outer hemisphere. Figure courtesy of Scienta Omicron AB.

3.1.4.1 Resolution

The resolution of the electron energy analyzer, ΔE, is given by:

$$\Delta E = \frac{sE_p}{2r} \tag{3.5}$$

where s is the width of the entrance slit of the analyzer, E_p is the pass energy and r is the radius of the electron energy analyzer.

For a given electron energy analyzer (a given r), the highest resolution is obtained using a narrow entrance slit and a low pass energy. The intensity depends on both of these parameters. Choosing a narrower slit and a lower pass energy will lower the intensity [93]. Thus, a compromise between intensity and resolution is needed.

In addition to the analyzer broadening of spectral lines, there will also be broadening from the photon source, lifetime broadening inherent in the sample and vibrational broadening. A photoelectron spectral lineshape is normally regarded to be of Voigt type, which is a convolution of a Gaussian part (instrumental broadening) and a Lorentzian part (lifetime broadening) [94]. In the measurements presented in this thesis, the Gaussian part of the lineshape dominates since the lifetime broadening is generally small.

3.1.5 Synchrotron radiation

To produce synchrotron radiation, an electron storage ring is used. The ring consists of an evacuated tube into which bunches of electrons are injected. The electron bunches travel in the ring at relativistic speeds. The ring is made up of straight segments with strong magnets (bending magnets) at the bending points. The bending magnets produce radiation of a broad energy range. On the straight segments, insertion devices such as undulators and wigglers are installed. Insertion devices consist of a periodic structure of dipole magnets that force the electrons of the storage ring to oscillate when passing. In a wiggler, the oscillations gives rise to a strong enhancement of the electromagnetic radiation in a broad bandwidth. An undulator produces very intense radiation in narrow energy bands. The produced radiation can be used to perform measurements. By varying the vertical distance between the dipole magnets (the undulator gap), the energy distribution of the produced radiation can be changed. The photons are delivered to a beamline, where a monochromator selects the wavelength (energy), for experimental use.

Synchrotrons provide high intensities with high brilliance, tuneable photon energies and a high degree of polarization of the photons. Synchrotrons produce radiation at a broad range of energies and measurements can be performed from the UV range up to more than 10 keV, depending on the beamline used. In this work, experiments have been performed at two synchrotron facilities; the MAX II storage ring at the MAX IV laboratory in Lund and BESSY II in Berlin.

3.1.5.1 I411

Most of the experiments presented here have been performed at the undulator beamline I411 [95, 96] at the MAX IV synchrotron facility in Lund. The beamline has a photon energy range between 50-1500 eV provided by a plane grating monochromator and the end station is equipped with a Scienta R4000WAL hemispherical analyzer. By small modifications of the end station, experiments can be performed on solid, liquid and gaseous samples.

The end station comprises, when equipped for studying solid state samples (as during the measurements presented in this thesis), several vacuum chambers connected with valves, as seen in Figure 3.4. Samples are inserted from atmosphere into a load lock chamber with a magnetic sample transfer rod. When the load lock chamber is evacuated, samples can be transferred to the next chamber which is referred to as the preparation chamber. In the preparation chamber, samples are transferred from the magnetic rod to a manipulator that can transfer the sample into measuring position in the analysis chamber. The preparation chamber and the analysis chamber are separated by a valve and when the pressure in the preparation chamber is sufficiently low, samples can be transferred to the analysis chamber. In the measurement position used in this thesis, the electron take off angle is 20-30 $^{\circ}$ and the X-rays impinge on

the sample at a 70-60 ° angle with respect to the sample surface. All chambers have turbo pumps to maintain the vacuum and during measurements, the base pressure is in the 10^{-8} mbar range. This system has been used for experiments in all the papers included in this thesis.

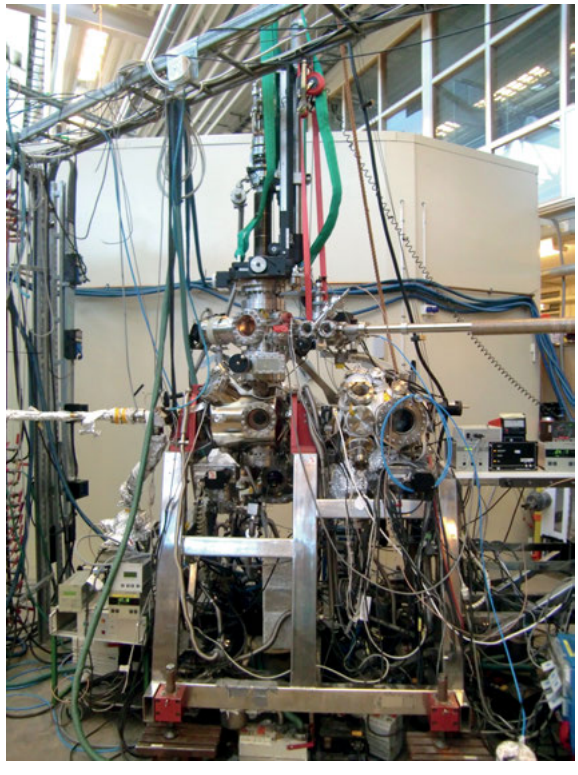

Figure 3.4. End station of beamline I411. From the left comes the beamline into the analysis chamber. On top the manipulator is mounted onto the preparation and analysis chambers. To the right is the magnetic transfer rod mounted onto the load lock chamber. The analyzer is behind the end station from this angle.

3.1.5.2 KMC-1/HIKE

KMC-1 is a HAXPES (Hard X-ray Photoelectron Spectroscopy) beamline situated on a bending magnet at the BESSY II synchrotron in Berlin [97, 98]. The beamline has a crystal monochromator with three different sets of crystals: Si(111), Si(311) and Si(422). The photon energy range is 2-12 keV and each set of crystals is suited for a specific range of energies. On the beamline is the endstation HIKE (HIgh Kinetic Energy) which is equipped with a hemispherical electron analyzer (Scienta R4000 10 keV), which is configured for detecting high kinetic energy electrons. A photo of the beamline is shown in Figure 3.5.

Measurements are usually done at a grazing incidence angle of the photon beam and the spectrometer is mounted at a 90 ° angle from the incident photon beam. This configuration maximizes the bulk sensitivity of the measurements. Measurements performed at this beamline are included in Paper V.

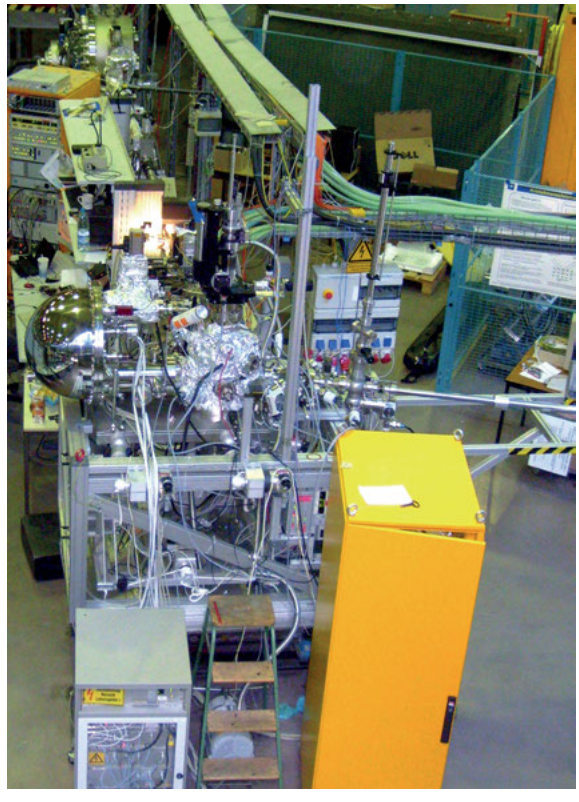

Figure 3.5. HIKE end station of beamline KMC-1. The beamline comes in from the top of the photo. At the right side is the magnetic transfer rod mounted on the load lock chamber. In the center of the end station is the analysis chamber and to the left is the hemispherical analyzer.

3.1.6 ESCA 300

An in-house ESCA 300 spectrometer [99], shown in Figure 3.6, using Al Kα radiation (1486.7 eV) was used for some measurements presented in this thesis. The photon source is a two stage high power electron gun accelerating electrons onto a water cooled rotating aluminium anode. The emitted radiation is further monochromatized using a quartz crystal monochromator. The instrument has a hemispherical electron analyzer with a radius of 300 mm from Scienta. For the measurements presented in this thesis an electron take

off angle of 90 ° has been used, but the instrument also allows for variable take off angle studies. The instrument has been used for measurements in Paper V.

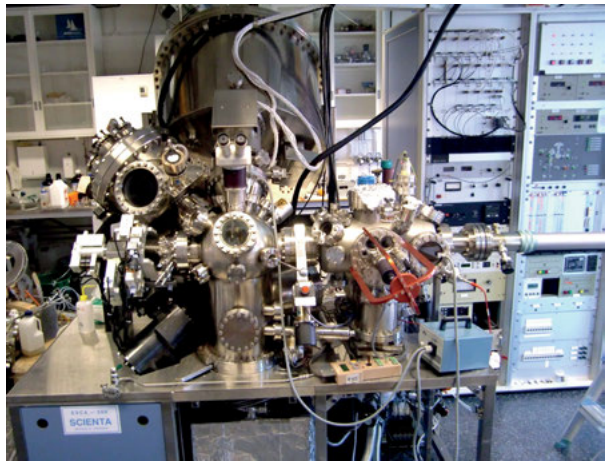

Figure 3.6. Photo of the in-house ESCA 300 instrument.

3.1.7 Energy calibration and intensity normalization

When studying energy level matching it is of great importance to have a reliable energy reference. For solid and metallic samples, the Fermi level is often used as a reference point by setting it a a binding energy of 0 eV. Throughout this thesis, the substrates used have been semiconductors (TiO_2 in Paper I-V and NiO in Paper VI), where the Fermi level can be hard to determine. Instead an internal energy reference from the substrates has been used for energy calibration. Measurements on TiO_2 have been energy calibrated by placing the $Ti2p_{3/2}$ core level peak at a binding energy of 458.56 eV [100]. The spectra measured with NiO as a substrate were energy calibrated by placing the O1s core level peak originating from NiO at 529.47 eV [35].

In order to compare signals from different samples, an intensity normalization is necessary. Two different approaches to this have been used in this thesis. In Paper I-II and V-VI, the intensities of the measured spectra have been normalized versus the substrate peaks (Ti2p, Ti3p or O1s for NiO). Another route, which has been used in Paper III-IV, is to normalize versus the background intensity in an energy region dominated by inelastic electrons from the substrate.

3.1.8 X-ray absorption spectroscopy

If the energy of an incoming X-ray photon matches the energy difference for an excitation, photon absorption can occur. In a simple picture this promotes

an electron from a core level to an unoccupied level leaving the atom with a core hole. The core hole will rapidly be filled by an electron from a higher state. During this process excess energy will be emitted in the form of Auger electrons or photons (fluorescence). Within the scope of this thesis, N1s-NEXAFS has been measured. For light elements as e.g. C, N and O, the Auger yield is more than two orders of magnitude higher than the fluorescence yield [101].

The Auger decay can be used for X-ray absorption spectroscopy (XAS) measurements, by scanning the photon energy over an absorption edge and measuring the number of emitted Auger electrons. If the absorption is studied close to an absorption edge, the technique is referred to as NEXAFS (Near Edge X-ray Absorption Fine Structure). Structures will appear in NEXAFS spectra at energies that relate to unoccupied electronic states. Transitions observed in X-ray absorption take place between states obeying the dipole selection rule, $\Delta l = \pm 1$ of the same atom and X-ray absorption thus is element specific. A deeper description of the processes involved can be found in various general and specialized textbooks [101, 102]. Calibration of the photon energy has been done by measuring a core level with first and second order light. The difference in kinetic energy equals the photon energy. NEXAFS measurements were performed at beamline I411 and are found in Paper I and III.

3.2 Solar cell characterization

In this section, the main techniques used to characterize DSCs will be presented in short.

3.2.1 UV-vis spectroscopy

The spectral behaviour of dye molecules is of great importance for the function of the DSC. This can be investigated by irradiating a sample with light in the UV-visible-NIR range and by the use of a grating and CCD detector measure the transmittance at different wavelengths. This allows for transmittance measurements of all wavelengths simultaneously. By using Lambert-Beer's law (see Equation 3.6), the extinction coefficient, ε, of the dye can be obtained, where A is the absorbance, c is the concentration and l is the length of the sample (the length of the cuvette). Absorbance , A, is related to transmittance, T, by $T = 10^{-A}$. Absorbance can also be measured on film, where Equation 3.6 is modified to account for surface coverage instead of concentration in solution.

$$A = \varepsilon c l \tag{3.6}$$

The absorbance can be linked to the light-harvesting efficiency, LHE, by using Equation 3.7, where I and I_0 are the intensities recorded with and without a sample present. LHE can also be referred to as absorptance.

$$LHE = 1 - \frac{I}{I_0} = 1 - 10^{-A} \tag{3.7}$$

3.2.2 IV

When comparing how well solar cells work, the power conversion efficiency of the cell is used. The efficiency can be obtained from a current-voltage (IV) measurement under simulated solar illumination with known power, P_{in}. From an IV-curve the short circuit current (J_{SC}) and the open circuit voltage (V_{OC}) can be obtained. The power conversion efficiency is then calculated using Equation 3.8, where P_{max} is the point of maximal power, P_{in} is the incident power and FF is the fill factor given by Equation 3.9.

$$\eta = \frac{P_{max}}{P_{in}} = \frac{J_{SC} V_{OC} FF}{P_{in}} \tag{3.8}$$

$$FF = \frac{J_{max} V_{max}}{J_{SC} V_{OC}} \tag{3.9}$$

An example of an IV curve of a D35 based DSC using an iodide based electrolyte is shown in Figure 3.7, where J_{max} and V_{max} determining P_{max} are indicated by the largest rectangle fitting under the IV curve. A solar simulator producing the AM1.5G solar spectrum is used to irradiate the cell. The intensity of the light is calibrated to 1000 Wm^{-2} (1 sun). To scan between short circuit and open circuit, the external load on the solar cell is changed from zero to infinity.

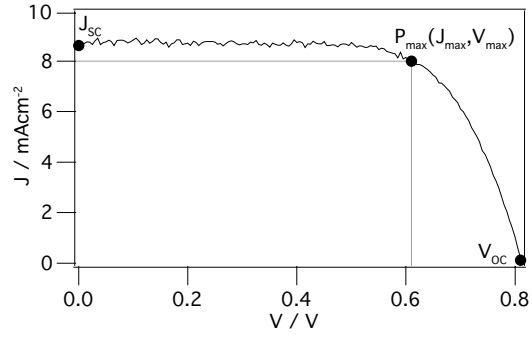

Figure 3.7. IV curve of a D35 based DSC with an iodide electrolyte.

3.2.3 IPCE

Spectral information on how well a solar cell converts photon flux to current at a given wavelength can be obtained by measuring the IPCE. The abbreviation IPCE stands for Incident Photon to Current Conversion Efficiency and can also be referred to as the external quantum efficiency (EQE). During an IPCE measurement, the solar cell is illuminated by monochromatic light and the photocurrent is measured as the wavelength is scanned using a monochromator. IPCE is calculated from the ratio of the number of electrons delivered by the cell to the number of photons incident onto the cell. The value can be used to evaluate the function of the solar cell. IPCE depends on the parameters in Equation 3.10

$$IPCE = LHE\phi_{inj}\phi_{reg}\phi_{coll} \tag{3.10}$$

where LHE is the light harvesting efficiency, ϕ_{inj} is the efficiency of electron injection into TiO_2, ϕ_{reg} is the efficiency of the regeneration of the oxidized dye molecules and ϕ_{coll} is the electron collection efficiency. An example of an IPCE spectrum of a DSC using D35 in combination with an iodide based electrolyte is shown in Figure 3.8.

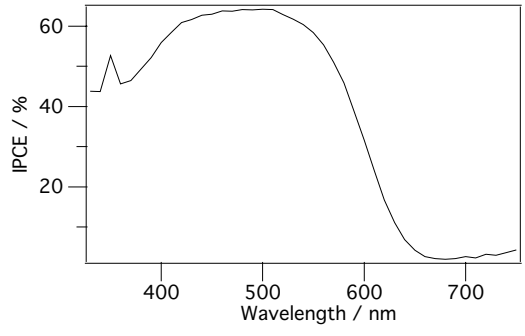

Figure 3.8. IPCE for a D35 based DSC with an iodide electrolyte.

3.2.4 Electron lifetime

Measuring the electron lifetime gives an estimation of how long time an electron can stay in the semiconductor after injection before it recombines with the oxidized dye molecule or the redox mediator. The electron lifetime is generally measured at open circuit. During the measurement the cell is illuminated by an LED. A small modulation of the bias voltage of the LED is applied and the response in photovoltage is recorded. The small modulation of the bias gives a single exponential decay of the photovoltage, which can be fitted to obtain the electron lifetime.

3.3 Sample preparation

The main focus of this thesis has been PES studies on electrodes used in DSCs. This section will therefore describe how samples were prepared for PES measurements. The preparation of complete solar cells is described elsewhere [10, 54].

All the samples were prepared on fluorine doped tin oxide (FTO) conducting glass (Pilkington TEC8 or TEC15). On the glass substrates, single layers of TiO_2 (Dyesol DSL 18 NR-T or Solaronix T37/SP) were screen printed at a thickness of 2-6 μm. In Paper V, DSL 18 NR-T electrodes were prepared by spin-coating and microbead electrodes by doctor blading. The NiO electrodes used in Paper VI, were prepared by screen-printing a 3 μm thick single layer of NiO. All electrodes were sintered at 450-500 °C for 30-60 min and left in the oven to cool down over night. Before dye-sensitization, the electrodes were cut to around 1 cm^2 and heated to 300 °C for 10 min. Before being immersed in the dye solutions, samples cooled down to around 80 °C. The sensitization time generally ranged from 4-18 h for the different projects. In Paper IV, sensitization time was used as a parameter and ranged from 1 s up to 24 h. After sensitization, the samples were rinsed with the solvent used in the dye bath and mounted onto the sample holder for transmission into the vacuum of the experimental setup.

4. Summary of results

The results are divided into two main parts depending on the kind of semiconductor electrode used. The first part focuses on samples having the common TiO_2 morphology. This part contains comparisons of single dyes, thermal treatment of dyes and co-adsorption of dyes and co-adsorbents. The second part describes different electrodes and includes a TiO_2 morphology suitable for use in solid state DSCs and mixed molecular layers on NiO.

The chemical structures of the organic dyes used in this thesis are shown in Figure 4.1. The metal-organic Ru-based dyes are shown in Figure 4.2 together with the co-adsorbent DPA and the adsorbents used in NiO based p-type DSCs are shown in Figure 4.3.

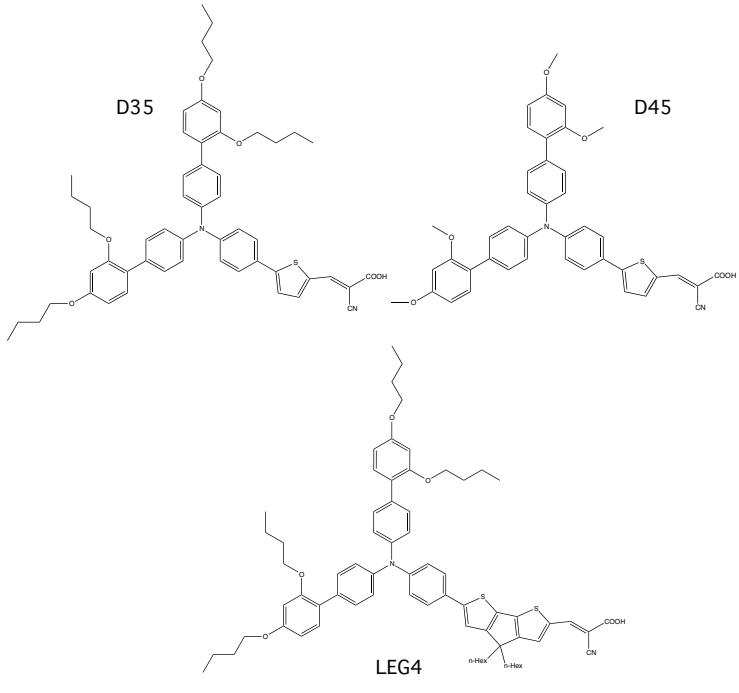

Figure 4.1. Chemical structures of the organic dyes used. D35 is used in Paper I, II, III and IV. D45 is used in Paper I and LEG4 in Paper V.

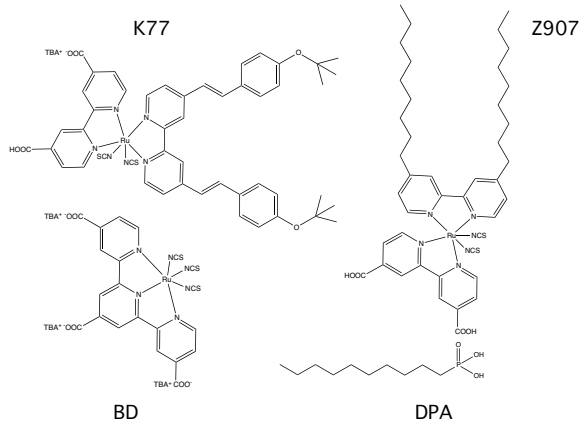

Figure 4.2. Chemical structures of the Ru based metal-organic dyes and the co-adsorbent DPA used. K77 is used in Paper II, Z907 in Paper III, BD in Paper IV and DPA in Paper III.

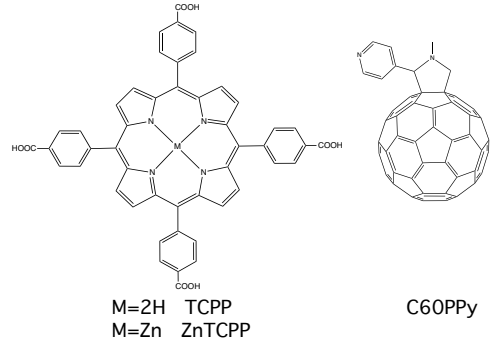

Figure 4.3. Chemical structures of the sensitizer molecules TCPP/ZnTCPP and C60PPy presented in Paper VI.

4.1 TiO_2 electrodes

This section contains comparisons of dyes with similar structures (Paper I), thermal treatment of dye-sensitized TiO_2 (Paper II) and co-adsorption giving mixed molecular layers at the TiO_2 surface (Paper III and IV).

4.1.1 Changes in the donor group of TAA based organic dyes

In Paper I, the two organic dye molecules D35 [51] and D45 [52] (see Figure 4.1) are compared when adsorbed to TiO_2. The only difference between the two dyes is the length of the alkoxy chains situated on the donor part of the molecules. Adding bulky groups on the donor part of the dye molecules can lead to lower recombination rate due to steric hindrance since molecules in the electrolyte are efficiently hindered from reaching the TiO_2 surface [103].

Less dye aggregation is another plausible effect of adding bulky groups on the donor part [104].

A summary of the solar cell performance of DSCs based on D35 and D45 with a Co-based liquid electrolyte is shown in Table 4.1. The results show that D35 gives higher numbers on all the investigated parameters. D35 also shows longer electron lifetimes than D45, as shown in Paper I. To deduce the reasons for this, a PES study together with theoretical DFT calculations was performed studying geometric (dye coverage and adsorption configuration) as well as electronic (energy level alignments) surface structure of the sensitized electrodes.

Table 4.1. *Summary of solar cell characteristics of D35 and D45 based DSCs. V_{OC} is the open circuit voltage, J_{SC} is the short circuit current density, FF is the fill factor and η is the power conversion efficiency.*

Dye	V_{OC} (V)	J_{SC} $(mAcm^{-2})$	FF	η $(\%)$
D35	0.86	9.43	0.69	5.6
D45	0.81	8.80	0.68	4.8

The S2p PES spectra shown in Figure 4.4(a) have been intensity normalized versus the substrate Ti2p signal, to give a measure of the surface coverage. The measurements show that the coverage of D45 is approximately 30 % higher than D35. Density functional theory (DFT) calculations indicate that the maximum D45 coverage is 47 % higher than for D35. This is something one to some extent might expect, since D45 is smaller than D35. The adsorption configuration of the dye molecules to the TiO_2 surface is another parameter that could affect the solar cell performance. This was experimentally studied from the N1s core levels, shown in Figure 4.4(b). By using Equation 3.4, the adsorption angle of the dye molecules to the TiO_2 surface can be estimated by comparing the N1s core level signals from the donor (TAA) and acceptor (CN) groups. The comparison showed that D35 and D45 have very similar adsorption configurations, with the dye molecules standing on the TiO_2 surface with the donor unit and alkoxy chains pointing away from the TiO_2. This is supported by DFT calculations which show that the most energetically favourable adsorption configuration is with the dye molecules standing on the TiO_2 surface.

To further investigate the geometry of the dyes at the TiO_2 surface, the C1s core level spectra shown in Figure 4.5 can be used. From the dye coverage estimation, we know that there is about 30 % more D45 on the surface as compared to D35. D35 has roughly 30 % more carbon atoms in its structure. Combining these, the C1s signal should be about the same from D35 and D45. In Figure 4.5, the C1s core level is measured with two different photon energies (758 and 454 eV). When measured with 758 eV, the C1s signal from D35 and D45 is very similar, when normalized versus the substrate. However, at 454 eV, the signal from D35 is 29 % stronger. We conclude from this that the

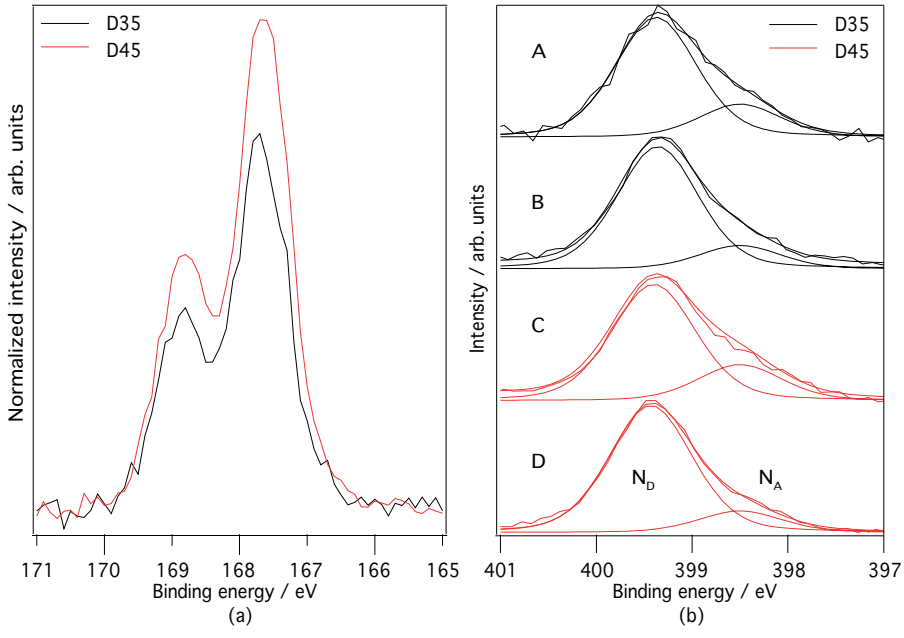

Figure 4.4. S2p (a) and N1s spectra (b) of D35 and D45. The S2p spectra are measured with a photon energy of 758 eV and intensity normalized versus the substrate Ti2p signal. The N1s spectra are measured with two different photon energies, A and C with 758 eV whereas B and D with 540 eV. The chemically shifted contribution from the donor and acceptor groups is indicated in the figure.

alkoxy chains of D35 are at the outermost surface, most probably forming an entangled layer. This layer may prevent electrons injected into the CB of TiO_2 from recombining with Co^{3+} complexes in the electrolyte, which ultimately leads to the longer electron lifetime observed for D35.

As previously discussed, also the energy level alignment will affect the performance of a DSC. To investigate this, the valence bands of D35 and D45 were measured using a photon energy of 150 eV, see Figure 4.6(a). The valence bands and the HOMO levels of the two dyes are, as seen in the figure, very similar. The unoccupied energy levels, probed by N1s-NEXAFS shown in Figure 4.6(b), reveals similarities between the two dyes. In Paper I, theoretical calculations are shown that support this. Thus, the energy levels of the dye molecules are not affected by the alkoxy chains on the donor group.

The main conclusion of Paper I is that the difference in solar cell performance of these rather similar dyes is attributed only to geometrical factors, i.e. the alkoxy chains of D35 preventing recombination and thereby enhancing the electron lifetime, leading to more efficient solar cells.

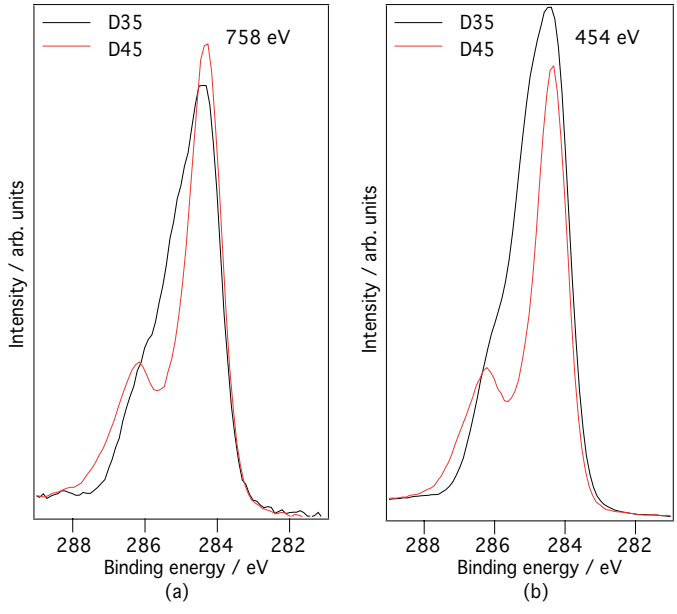

Figure 4.5. C1s spectra measured with photon energies of 758 eV (a) and 454 eV (b).

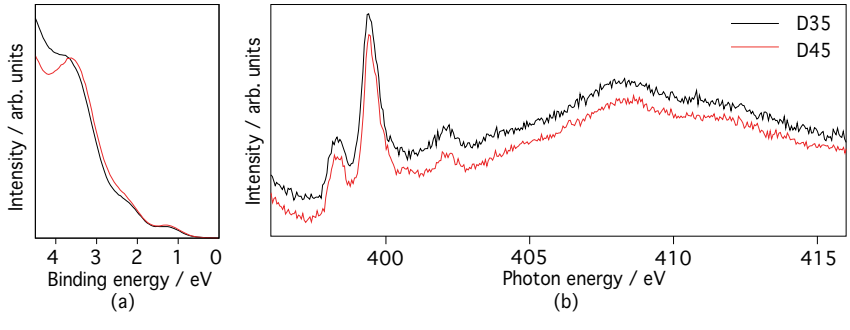

Figure 4.6. Valence levels measured with a photon energy of 150 eV (a) and N1s-NEXAFS spectra (b) of D35 and D45 on TiO_2.

4.1.2 Effect of thermal treatment on dyes

Dye molecules are often subjected to elevated temperatures, both during the manufacturing of DSCs as well as during operation. Liquid-based DSCs can use a thermoplastic for assembling the electrodes. The thermoplastic needs to be heated to 100-130 °C in order to seal the electrodes together [105–107]. One method to prepare ssDSCs utilizes infiltration of the hole conductor in its

molten form [108], which allows for thicker TiO_2 films with efficient pore filling. In operation, the internal temperature of a DSC normally reaches 40-50 °C but during extreme weather conditions it can reach up to 70 °C [109, 110]. Studies have shown that heat-treatment of DSCs lowers their performance [111–116]. Thermal stability of dyes is of great importance for the function of DSCs. Paper II focuses on the effects of thermal treatment of the dyes D35 and K77 [63] (see their chemical structures in Figure 4.1 and 4.2) both in terms of DSC performance and on the molecular scale using PES. Dye-sensitized electrodes were heat-treated in ambient air for 5 min at 100, 150 and 200 °C. These electrodes were then compared with pristine (non heat-treated) electrodes. A summary of the solar cell characteristics of DSCs comprising these electrodes with an I^-/I_3^--based electrolyte is shown in Table 4.2.

Table 4.2. *Summary of solar cell characteristics of the heat-treated DSCs. V_{OC} is the open circuit voltage, J_{SC} is the short circuit current density, FF is the fill factor and η is the power conversion efficiency. From Paper II.*

Sample	V_{OC} (V)	J_{SC} $(mAcm^{-2})$	FF	η (%)
D35				
Not heated	0.85	8.09	0.64	4.4
100 °C	0.84	7.20	0.65	4.0
150 °C	0.78	4.45	0.66	2.3
200 °C	0.48	0.22	0.56	0.1
K77				
Not heated	0.72	9.25	0.68	4.5
100 °C	0.69	8.19	0.70	4.0
150 °C	0.62	4.21	0.68	1.8
200 °C	0.50	0.95	0.66	0.3

The power conversion efficiencies drop with over 90 % for both dyes when heat-treated at 200 °C. PES was used as a tool to understand the effects of the heat-treatment at the molecular level.

Figure 4.7 shows the N1s (a) and S2p (b) spectra of the D35 samples. The N1s core level spectra were measured using a photon energy of 535 eV and curve fitted using two components, N_A and N_D as previously discussed, as shown in the figure. No differences in total N1s signal (versus Ti3p substrate signal) are detected as a consequence of the heat-treatment. The relative ratio of N_A to N_D also remains unaffected throughout the series. The S2p spectra shown in Figure 4.7(b) reveals that two spin-orbit split components are needed to curve fit the spectra, even though D35 has a single sulfur atom in the structure. The doublet at the highest binding energy is referred to as S_L (linker) and the smaller doublet at lower binding energy as S_E (extra). The presence of the extra doublet has been observed earlier for similar dyes [117] and can, as for metal-organic dyes be explained by a mixture in adsorption configurations to the TiO_2 surface [100]. S_L is attributed to dye molecules adsorbing to TiO_2

standing up while S_E is attributed to dye molecules adsorbing with a large angle to the surface normal. The angle allows for interaction between the sulfur of the dye and the TiO_2 surface resulting in the large chemical shift observed. The total S2p signal remains constant versus Ti3p for all samples. However, the relative intensity of S_E increases when heat-treated (at 200 °C it is double as compared to pristine) and thus, S_L decreases correspondingly. This indicates that the adsorption configuration of a fraction of the D35 molecules is altered by heat-treatment, which may have important consequences for the energy conversion process.

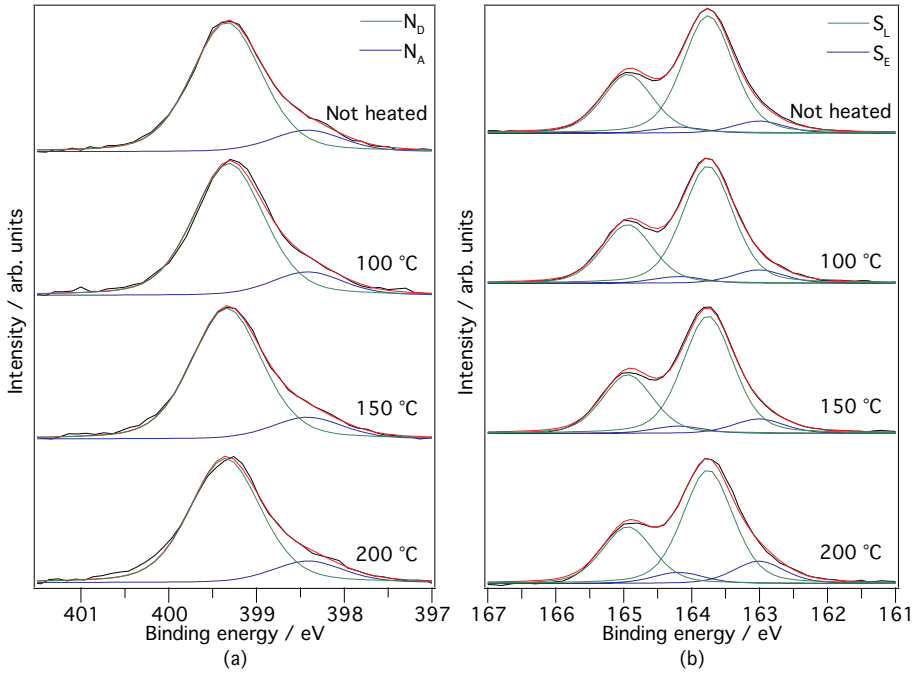

Figure 4.7. N1s (a) and S2p (b) spectra of the heat-treated D35 samples. N1s measured with a photon energy of 535 eV and S2p with 454 eV.

Figure 4.8 shows the N1s (a) and S2p (b) spectra of the K77 samples. The N1s spectra measured with a photon energy of 535 eV are curve fitted using four peaks: N_{TBA} from the *tert*-butylammonium (TBA) counter ion, N_P from the bipyridine whereas the thiocyanate ligands (NCS) give rise to two peaks; N_{NCS1} and N_{NCS2}. Ru-based dyes have previously been observed to interact with the substrate via the thiocyanate ligands, giving rise to two components in the signal from both nitrogen and sulfur from the ligands [100, 118]. The total N1s intensity (versus the substrate) decreases progressively when heat-treated. The intensity of N_{TBA} and N_P remains constant, whereas the total intensity from the thiocyanate nitrogen (N_{NCS1} and N_{NCS2}) decreases, indicat-

ing a partial loss of thiocyanate ligands. Similar effects are also observed in the S2p spectra.

The S2p spectra measured with a photon energy of 454 eV are shown in Figure 4.8(b). In the chemical structure of K77, sulfur is only present in the thiocyanate ligands. However, five spin-orbit split components are necessary to curve fit the spectra. The two at the lowest binding energies are assigned to the thiocyanate ligands, similar to the N1s spectra [100, 118]. The remaining three are assigned to various sulfurous oxides; SO_4 at a binding energy of 168 eV, SO_3 at 166.5 eV, whereas the contribution at 164 eV is unclear and referred to as SO_X. The positions of these peaks are in agreement with what has previously been seen for sulfurous oxides on metals and metal oxides [119–122]. The total S2p signal remains constant throughout the heat-treatment, but the total intensity from NCS (S_{NCS1} and S_{NCS2}) decreases and the total intensity from the sulfurous oxides increases progressively with increasing heat-treatment temperature. This indicates that part of the thiocyanate ligands detach from the molecules as a consequence of heat-treatment and during this process, nitrogen is lost whereas sulfur adsorbs to the TiO_2 surface as sulfurous oxide.

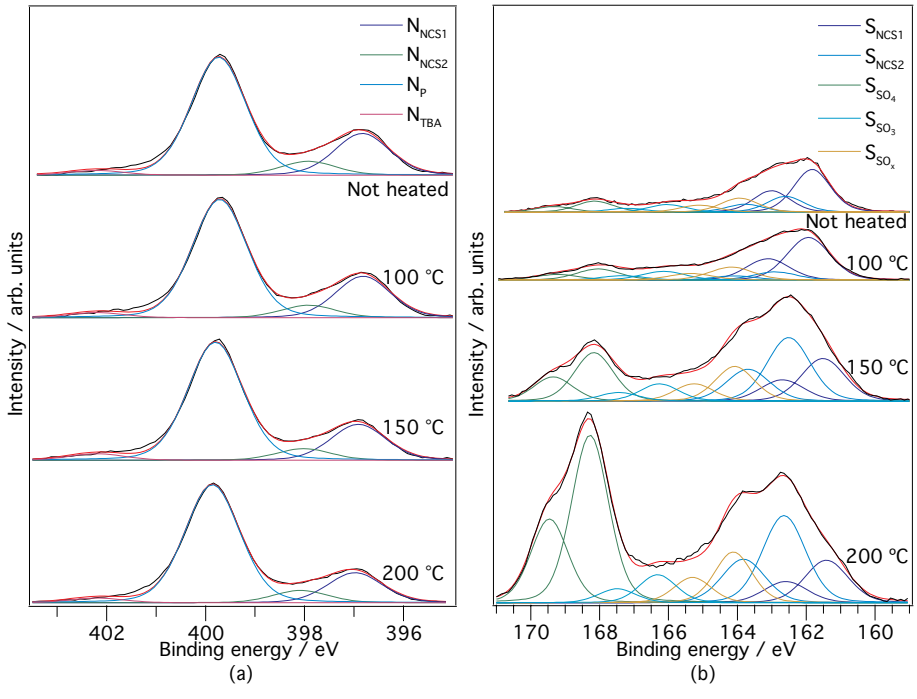

Figure 4.8. N1s (a) and S2p (b) spectra of the heat-treated K77 samples. N1s measured with a photon energy of 535 eV and S2p with 454 eV.

Figure 4.9 shows the outermost parts of the valence bands of the D35 (a) and K77 (b) samples. The vertical lines in the figure indicate the position of the HOMO level in each sample. For D35, the valence bands were measured using a photon energy of 100 eV. A gradual shift in binding energy of the HOMO level is observed when heat-treated. The maximal shift is +0.2 eV when heat-treated at 200 °C. The shift is ascribed to the change in adsorption configuration previously discussed. The HOMO level of D35 is mostly located around the donor part of the molecule with contributions from the phenyl groups and alkoxy chains [51, 117, 123]. This positioning of the HOMO level explains why the binding energy of it is affected by a change in adsorption configuration.

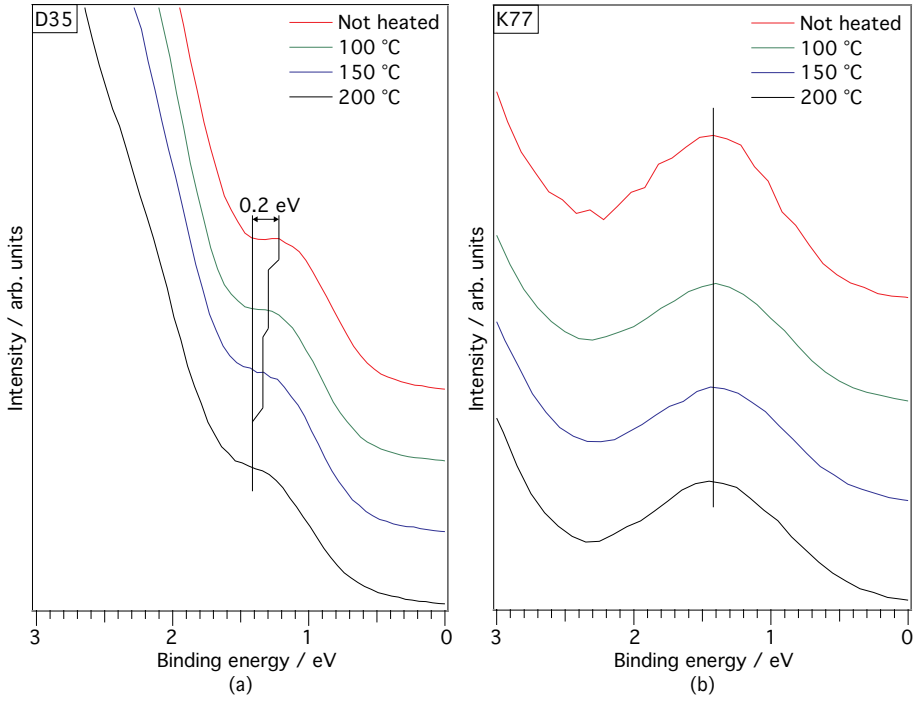

Figure 4.9. The outermost parts of the valence band of heat-treated D35 (a) and K77 (b). D35 samples measured with a photon energy of 100 eV and K77 with 454 eV. The connected vertical lines show the position of the HOMO level in each sample.

The binding energy of the HOMO level of the K77 samples is not affected by heat-treatment, as indicated in Figure 4.9(b). The HOMO level of K77 (and other Ru-based dyes) is to a large extent located on the ruthenium atom [67], which means that it is quite stable. The HOMO level however gets less pronounced from heat-treatment, indicating a loss of HOMO level electrons, which will have negative impact of the solar cell performance.

The main observable of Paper II is the severe decrease in power conversion efficiency when heat-treated. For D35, we conclude that the reason for this decrease is a change in molecular configuration of the dye molecules at the surface which affects the energy levels and their alignment, which probably increases the recombination in the DSC. For K77 however, the explanation of the decrease in power conversion efficiency is that the dye molecules actually break from the heat-treatment and that the products cannot function as sensitizers.

4.1.3 Co-adsorbents in the molecular layer

There are several approaches on how to produce more efficient DSCs, e.g. optimization of the constituting parts of the DSC and combinations of constituents. Many studies have shown that the power conversion efficiency can be increased by the addition of co-adsorbents in the dye bath solution [124–142]. The knowledge of how dye molecules are affected by the addition of co-adsorbents is however limited. In Paper III, we have investigated how the metal-organic dye Z907 [64] (at a constant concentration of 300 μM in solution) is affected by addition of *n*-decylphosphonic acid (DPA) in varying concentrations (see Figure 4.2 for chemical structures) at a molecular level using PES. Another important route towards more efficient DSCs is to enhance the light absorption. It can e.g. be done by synthesizing new dyes or by co-adsorbing several dyes with complementary light absorption properties. The latter has recently shown to be very successful and the most efficient DSC today comprises two different co-adsorbed dye molecules [9]. The co-adsorption of a dye with other dye molecules has been investigated in Paper III and IV, where the metal-organic dyes Z907 and Black dye (BD) [59] (Figure 4.2) have been co-adsorbed with D35 (see Figure 4.1). Z907 and D35 were co-adsorbed from different relative concentrations in solution, while for the mixture of BD:D35, two series were prepared; the first having a constant concentration of BD (500 μM) and varying D35 concentrations and the second series utilizing constant concentrations of BD:D35 (400 μM:200 μM), i.e. a ratio of 1:0.5, for sensitization times ranging from 1 s to 86.4 ks (24 h).

The dye molecules are expected to adsorb to the TiO_2 surface via the anchoring groups. As shown in the S2p spectra presented in Paper III and IV, both Z907 and BD additionally shows signs of interacting with the TiO_2 surface via the thiocyanate ligands, as also observed for K77 in Paper II. Figure 4.10 shows the S2p spectra of Z907 co-adsorbed with DPA and with D35 as well as BD co-adsorbed with D35. The curve fit of the Z907:DPA (Figure 4.10(a)) samples illustrates the interaction to TiO_2 via the thiocyanate ligands by the presence of the $S2p_B$ component ($S2p_A$ is the contribution expected from the ligand). The interaction through the thiocyanate ligands of Z907 is affected both by the addition of DPA and D35 (Figure 4.10(a, b)).

DPA at high concentrations increases this interaction, while D35 already at low concentrations removes the interaction, i.e. the S2p$_B$ contribution disappears when D35 is present at the surface. For BD, the S2p$_B$ contribution is also affected by the addition of D35, as shown in Paper IV, for all samples having a sensitization time longer than 1 ks (Figure 4.10(c) and (d)). For shorter times, the dye coverage is low, so no changes are observed. Longer sensitization times and higher concentrations of D35 in the sensitization solution gives a S2p$_B$ contribution that is around a third of the initial value. Thus, BD is not affected as much as Z907 by the addition of D35 even though similar effects are observed. This is most likely due to the fact that BD has three thiocyanate ligands while Z907 only has two.

The co-adsorption of Z907:D35 and BD:D35 is schematically illustrated in Figure 4.11. Green circles illustrate adsorption sites on the TiO_2 surface, red ovals are D35 and the blue symbols illustrate Z907 and BD respectively. The color of the attached triangles and half circles illustrate the mode of interaction between the thiocyanate ligands and the TiO_2 surface. For Z907, red triangles illustrate molecules interacting through the thiocyanate ligands, yellow triangles show molecules not having this interaction and green triangles show molecules with exposed thiocyanate ligands (less attenuation). Similarly, red half circles for BD indicates interaction while yellow means no interaction through the ligands to the TiO_2 surface. The co-adsorption of Z907:D35 (a) indicates the gradual change in adsorption configuration mentioned above by the disappearance of the interaction between thiocyanate and TiO_2 (red triangles) and the appearance of the less attenuated ligand signal (green triangles). For BD:D35 (b), the partial adsorption configuration change is illustrated by the suppression of the interaction between ligand and TiO_2 (red half circle) and the increase of the non-interacting component (yellow half circle).

The Ru3d spectra shown in Paper III show that the amount of Z907 at the surface decreases when D35 is added. This in combination with the change in adsorption configuration, as discussed above, instead indicates that the Z907 molecules reorient at the surface, leaving the thiocyanate ligands more visible. The same is true for BD, but the effects are smaller than for Z907.

To quantify the amounts of Z907 and DPA at the surface, the Ru3d (only present in Z907) and P2p (only DPA) spectra were investigated using PES, as shown in Paper III. The quantification is illustrated graphically, in terms of atomic percentage of Ru and P as function of DPA concentration in the dye solution, in Figure 4.12. Also included in the figure is the atomic percentage of Ru plus a sixth of the atomic percentage of P, which interestingly results in an almost linear behaviour. This indicates that Z907 is replaced by DPA at the surface and that each Z907 molecule is replaced by six DPA molecules.

The HOMO level of the co-adsorbed systems was measured to study the energy level alignment in the system. In the case of Z907 and DPA, no shifts of the HOMO level were detected, as shown in Paper III. For Z907 and D35 however, a shift of approximately -130 meV was seen for the Z907 contribution

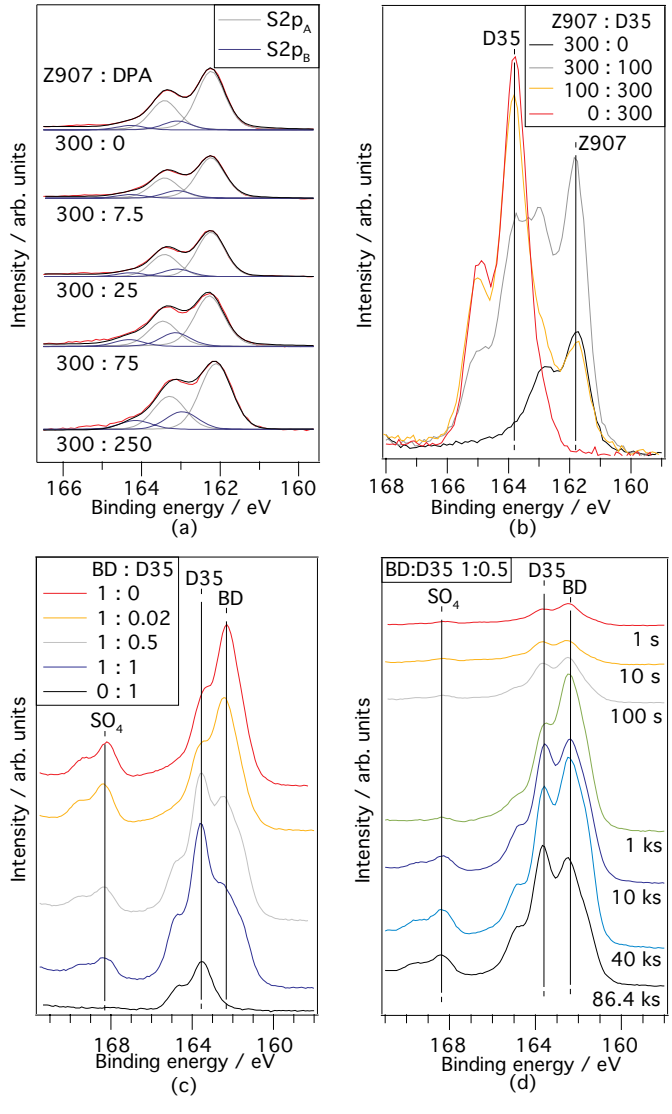

Figure 4.10. S2p spectra of the co-adsorbed samples. (a) shows Z907 with different concentrations of DPA, (b) Z907 with D35, (c) BD with D35 at different concentrations and (d) BD with D35 at different sensitization times. The Z907:DPA samples are shown with their curve fits showing the two spin-orbit split doublets. All spectra were measured using a photon energy of 454 eV. (a) and (b) come from Paper III while (c) and (d) come from Paper IV.

when D35 was added, as shown by the vertical lines in Figure 4.13(a). The HOMO level is predominantly located on the Ru atom with some contribution from the NCS ligands, causing the HOMO level spectra to be dominated by Ru4d character [66, 67]. The Ru3d core level showed a shift of the same order

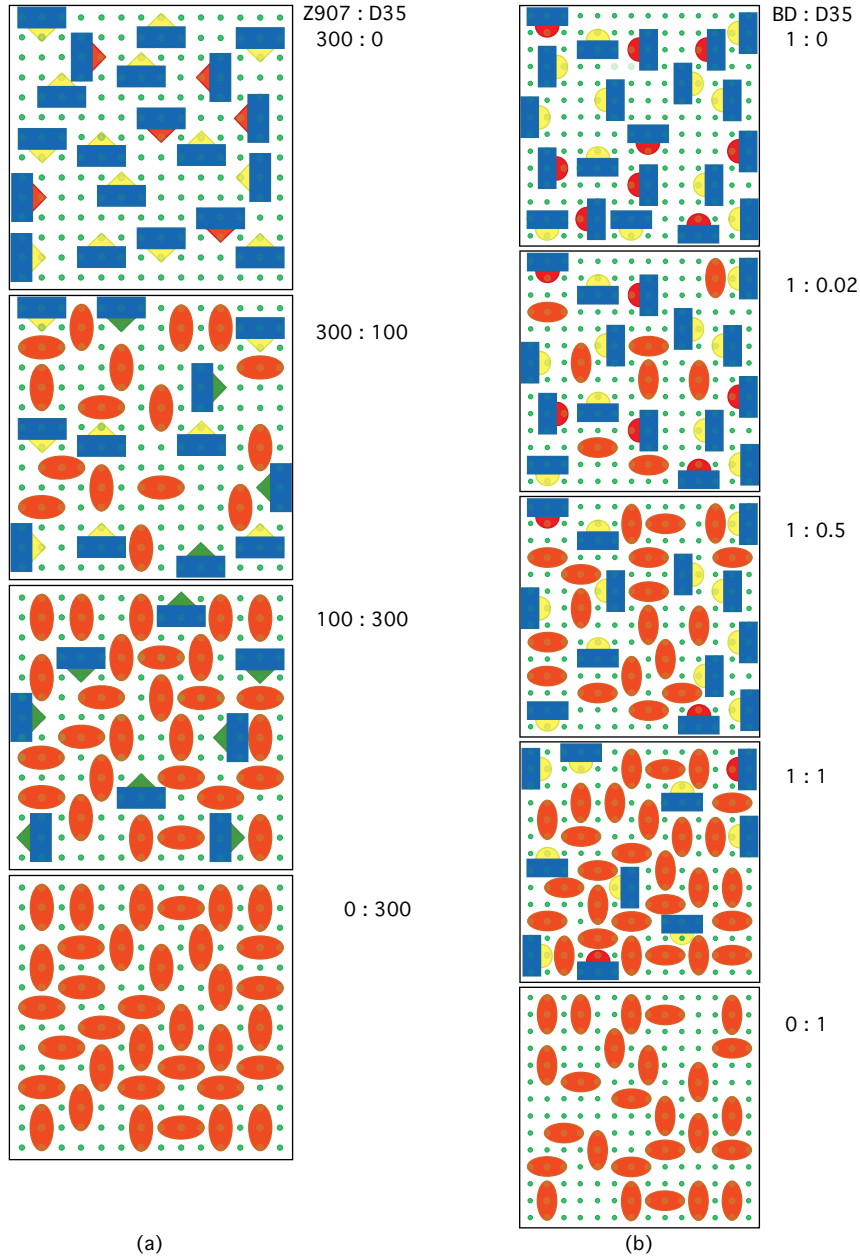

Figure 4.11. Schematic illustration of the adsorption to TiO_2. The green circles illustrate adsorption sites on a TiO_2 surface, the red ovals are D35 and the blue symbols are Z907 and BD respectively, where the color of the attached triangles and half circles illustrate interaction between NCS and TiO_2, as discussed above. (a) shows the co-adsorption of Z907 and D35 from Paper III. (b) shows the co-adsorption of BD and D35 at a constant BD concentration from Paper IV.

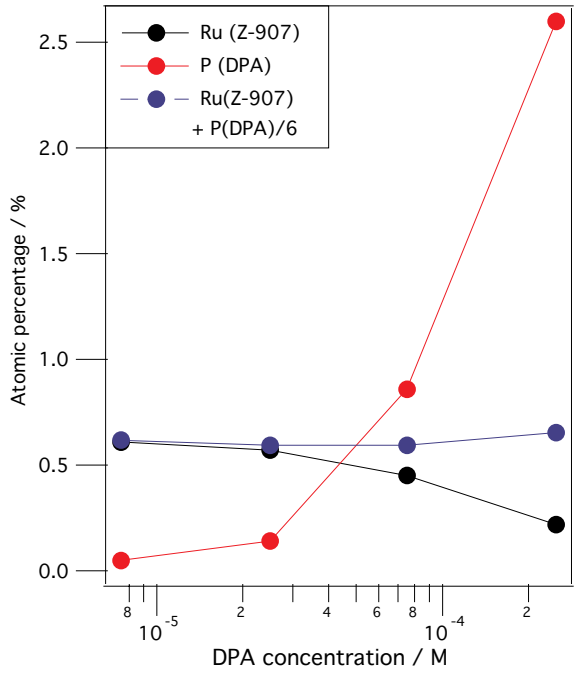

Figure 4.12. Atomic percentages of Ru and P together with the sum of the atomic percentage of Ru and a sixth of P plotted versus the DPA concentration in dye solution. Based on measurements using Al Kα radiation.

when D35 was added. For the BD:D35 samples, no shifts of the HOMO level or the Ru3d core level could be detected, as shown in Figure 4.13(b). The reason for the different behaviour of Z907 and BD when co-adsorbed with D35 is most likely due to the difference in adsorption configuration changes, i.e. the suppression of the interaction between NCS and TiO_2.

As a summary, DPA at high concentrations affects the interaction between Z907 and the TiO_2 surface in a non-beneficial way from the perspective of DSC function. However, the energy level alignment between dye and TiO_2 is not affected by the presence of DPA. Co-adsorbing Z907 with D35 induces changes in the adsorption configuration of Z907, suppressing the interaction between the thiocyanate ligands and the TiO_2 surface. At the same time, changes in the electronic structure are detected for Z907 by the means of core level and HOMO level shifts. This is presented in Paper III. For BD:D35, the interaction between thiocyanate ligands and TiO_2 is suppressed but to a smaller extent compared to Z907. No shifts in energy level alignment were detected, as presented in Paper IV. The changes at a molecular level indicate that the co-adsorption process takes place in a collaborative way both for Z907 and BD. Common for all the samples is that an excess of D35 to Ru-dye is al-

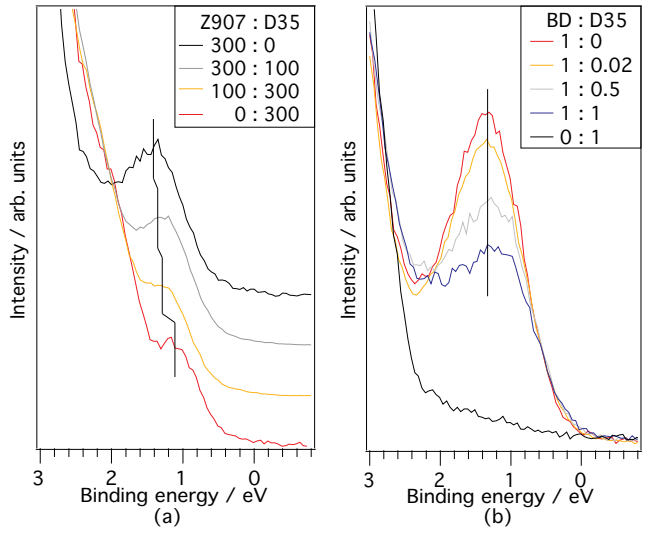

Figure 4.13. The outermost part of the valence band of the Z907:D35 (a) and BD:D35 samples (b). The vertical lines show the position of the HOMO level. The spectra in (a) were measured using a photon energy of 150 eV and (b) 454 eV.

ways observed at the TiO_2 surface as compared to the concentration ratio in sensitization solution.

4.2 Other semiconductor electrodes

In this section, different substrates have been used. In Paper V, a mesoporous TiO_2 morphology showing promising results for the use in solid state DSCs has been investigated. Paper VI focuses on adsorption of different molecules to the p-type semiconductor NiO, ultimately leading to mixed molecular layers on NiO.

4.2.1 TiO_2 morphology for solid state DSCs

The function of the solid state DSC (ssDSC) is dependent on the ability of the hole conductor to penetrate into the pores of the semiconductor. This limits the thickness of the TiO_2 film and thereby also the light harvesting efficiency. As of today, this is one of the greatest challenges before truly high efficiency ssDSCs can be realized. For this reason, a lot of research on different TiO_2 morphologies, e.g. nanotubes [143], ordered nanorods [144] and mesoporous single crystals [145] has been done. However, the use of different morphologies often come at the expense of lower accessible surface area per unit thickness of the TiO_2 film. Therefore, the interest for "normal" mesoporous films with high surface area and controllable and changeable pore sizes has grown

lately. In liquid-based DSCs, a microbead (MB) TiO_2 morphology comprising sub-μm-μm anatase TiO_2 particles has shown great promise with power conversion efficiencies of over 10 % [146–148]. The size of the pores and the overall porosity of an MB electrode can be changed in a controlled way, making MB a good candidate for the use in high efficiency ssDSCs. Furthermore, the larger size of the microbeads as compared to the normally used TiO_2 particles (around 20 nm) increases the diffuse light scattering in the electrode paving the way to higher LHE. In Paper V, we compared standard TiO_2 (Dyesol DSL 18 NR-T, referred to as DSL in the text) to MB as well as the performance of ssDSCs comprising these electrodes sensitized by LEG4 [53, 54] (see Figure 4.1) with spiro-OMeTAD as a hole conductor.

A summary of the solar cell performance of MB and DSL based ssDSCs is shown in Table 4.3. DSL has a higher J_{SC}, FF and power conversion efficiency while MB produces the highest open circuit voltage. The power conversion efficiency of the MB based ssDSC was the highest reported using a different TiO_2 morphology.

Table 4.3. *Summary of solar cell characteristics of ssDSCs comprising MB and DSL working electrodes sensitized with LEG4 and using spiro-OMeTAD as hole conductor. V_{OC} is the open circuit voltage, J_{SC} is the short circuit current density, FF is the fill factor and η is the power conversion efficiency.*

Sample	V_{OC} (V)	J_{SC} $(mAcm^{-2})$	FF	η (%)
MB	0.86	7.9	0.52	3.5
DSL	0.81	10.3	0.70	5.8

To understand why MB gives a higher open circuit voltage, the un-sensitized electrodes were studied using PES. Figure 4.14 shows the Ti2p core level measured with photon energies from 758 - 6000 eV, i.e. from surface to bulk sensitive measurements. As can be seen, all spectra are similar indicating both that each sample is homogeneous in itself and that MB and DSL are very similar, i.e. no difference in the amount of Ti^{3+} is seen.

As shown in Paper V, the valence bands probed with photon energies from 1487-6000 eV show the same behaviour. However, when studying the valence bands with a lower photon energy (150 eV) as shown in Figure 4.15, we observe differences. The valence band edge is on the left hand side of the figure, meaning that the features observed above it are trap states in the band gap. There are significantly more trapped electrons in the DSL film as compared to MB. In the PES measurements, these states are occupied but in a DSC they can be depleted in contact with the dye and the hole conductor. Thus, in a DSL DSC there are significantly more (empty) trap states to fill with electrons injected from the dye as compared to MB DSCs. This is also seen from the longer electron transport time for DSL presented in Paper V. In the paper, we also show evidence for complete pore filling of spiro-OMeTAD in the thicker MB film.

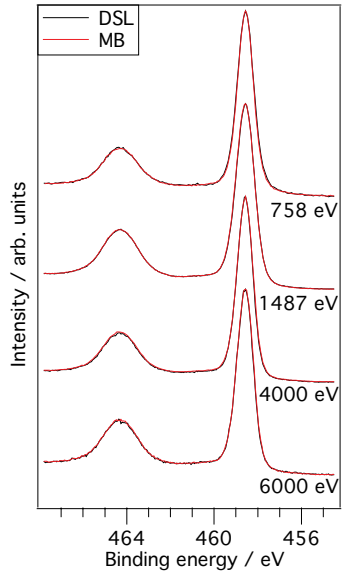

Figure 4.14. Ti2p core levels of MB and DSL TiO_2 electrodes measured with different photon energies. The spectra are strikingly similar.

The conclusions of Paper V is that the lower number of trap states in MB causes the higher open circuit voltage and shorter electron transport time within the TiO_2 film and that the MB morphology shows great promise for the use in ssDSCs providing thicker TiO_2 films with good hole conductor pore filling.

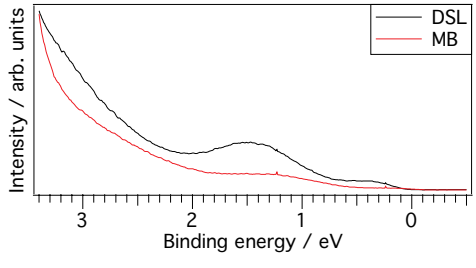

Figure 4.15. Outermost parts of the valence bands of MB and DSL TiO_2 measured with a photon energy of 150 eV. The valence band edge is at the left in the figure, so the features above it are trap states in the band gap.

4.2.2 Towards mixed molecular layers for the use in p-type DSCs

The power conversion efficiency of p-type DSCs is much lower than for their n-type counterpart [10]. One reason for this is the fast recombination after hole injection from the sensitizer into the valence band of NiO [149]. One way of lowering the recombination is by synthesizing new tailored sensitizers,

mostly by distancing the electron acceptor unit from the p-type surface leading to a longer lifetime of the excited state [150, 151]. Porphyrin dyes have shown high power conversion efficiencies in n-type DSCs [152] and the fast charge transfer process from porphyrins to C60 derivatives [153–157] suggested that this combination could be used to inhibit recombinations and thereby increase the power conversion efficiency of the DSC. The C60 derivative is expected to coordinate to the metal (most commonly Zn) center of the porphyrin via a nitrogen atom in its structure. In Paper VI, we investigated the interaction between two porphyrins (TCPP and ZnTCPP) with the fullerene derivative C60PPy (see Figure 4.3 for chemical structures). Samples were prepared by sequential sensitization of NiO in porphyrin and fullerene. The samples are referred to by the order of sensitization, e.g. ZnTCPP/C60PPy means that the NiO was sensitized first by ZnTCPP and then by C60PPy. The investigation was carried out on DSC performance as well as by PES measurements on sensitized NiO electrodes.

A summary of the solar cell characteristics of the DSCs comprising ZnTCPP is presented in Table 4.4. The data in the table are an excerpt from Paper VI. ZnTCPP/C60PPy outperforms the other samples, giving the most efficient solar cell. To understand why, sensitized NiO films were studied using PES.

Table 4.4. *Part of the solar cell characteristics of p-type DSCs presented in Paper VI. V_{OC} is the open circuit voltage, J_{SC} is the short circuit current density, FF is the fill factor and η is the power conversion efficiency.*

Sample	V_{OC} (V)	J_{SC} $(mAcm^{-2})$	FF	η $(\%)$
ZnTCPP	0.12	0.5	0.40	0.02
ZnTCPP/C60PPy	0.16	1.5	0.38	0.09
C60PPy/ZnTCPP	0.13	1.0	0.37	0.05

The N1s core level spectra of the NiO based samples together with an unsensitized NiO electrode are shown in Figure 4.16 with their corresponding curve fits. All samples containing a porphyrin, i.e. all but C60PPy and NiO are strikingly similar with two nitrogen species, as seen from the curve fits. The peak at a binding energy of 400.5 eV is assigned to protonated nitrogen, while the peak at 398.5 eV comes from de-protonated nitrogen. These peaks are characteristic for metal-free porphyrins [158], e.g. TCPP. For ZnTCPP, a single peak in the N1s spectra is expected. The presence of two peaks suggests that the Zn atom is detached from the molecule and that part of the nitrogen atoms get protonated instead [159]. However, for ZnTCPP/C60PPy a third feature is observed at a binding energy of 399.5 eV, and it is assigned to Zn ligated nitrogen [160]. This suggests that the adsorption configuration of ZnTCPP changes when C60PPy is added.

Zn3d was studied by measuring the valence band of the samples, as shown in Paper VI, and subtracting the valence band of NiO from the sensitized samples. The subtraction is shown in Figure 4.17. Zn3d appears at a binding

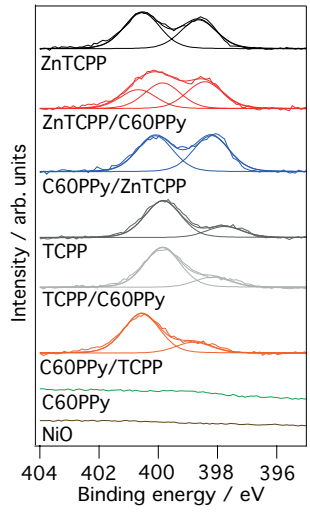

Figure 4.16. N1s spectra of the NiO based samples measured with a photon energy of 540 eV.

energy of 10.6 eV for all samples containing ZnTCPP. The binding energy distance between C1s and Zn3d is indicative of neutral zinc, suggesting that the Zn binds to the NiO surface and reduces to Zn^0. This also indicates that zinc is removed from the porphyrin molecule.

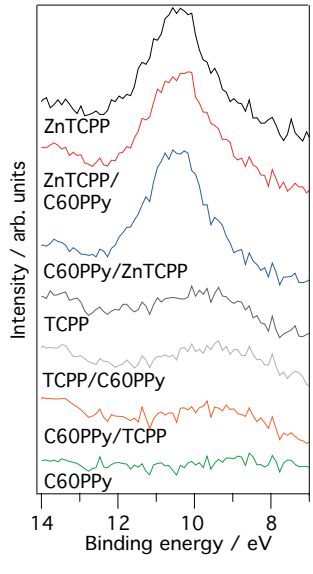

Figure 4.17. Subtraction of the valence band of un-sensitized NiO from the sensitized samples, to visualize the Zn3d core level. Based on measurements performed with a photon energy of 454 eV, presented in Paper VI.

In Paper VI, the O1s core level spectra of all samples are shown. To deduce the effects of sensitization, a spectrum subtraction was performed in a similar manner as for the valence bands. The result of the subtraction is displayed in Figure 4.18. All samples containing porphyrin show two features in the subtracted spectra. The one at higher binding energy is assigned to protonated oxygen, while the one at lower energy correspondingly to de-protonated oxygen [159]. ZnTCPP/C60PPy shows a significantly higher -OH signal than the other samples. Given the surface sensitivity of PES, this indicates that the carboxylic acid groups are most visible, i.e. pointing outwards, for the ZnTCPP/C60PPy sample as compared to the others. The interpretation is that ZnTCPP and TCPP on their own adsorb to NiO in a lying down configuration, i.e. using a majority of the anchoring groups causing the molecules to adsorb flatly to NiO, which is supported by FT-IR measurements presented in Paper VI. Adding C60PPy causes some of the ZnTCPP molecules to instead adsorb in a standing up configuration with some of the anchoring groups now pointing outwards, accounting for the increased -OH feature in the subtracted spectra. This further strengthens the adsorption configuration change for ZnTCPP/C60PPy.

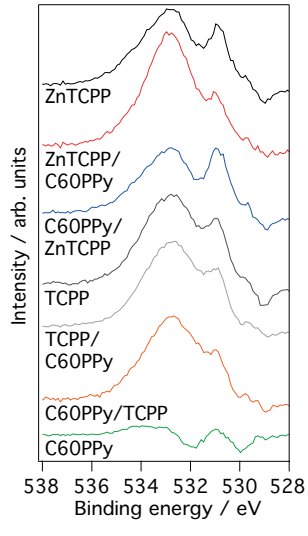

Figure 4.18. Subtraction of the the O1s core level of un-sensitized NiO from the sensitized samples, to show oxygen species originating from the sensitization process. Based on measurements with a photon energy of 758 eV, presented in Paper VI.

All together, the addition of C60PPy to ZnTCPP induces an adsorption configuration change of ZnTCPP allowing C60PPy to coordinate to it. The outcome of this is faster charge transfer and slower recombination, as shown in Paper VI, ultimately leading to a more efficient DSC.

5. Outlook

The work presented in this thesis shows that PES is a useful tool to study the sensitized working electrode of DSCs. The main focus has been to study the geometrical and electronic surface structure of single dyes and mixed molecular layers at mesoscopic oxide interfaces.

To further understand the effects of mixed molecular layers in DSCs, more thorough investigations of co-adsorbed systems would be beneficial. By expanding the study to also include other kinds of dye molecules, e.g. porphyrins, metal-organic dyes based on other metals than Ruthenium and different organic dyes, the process of co-adsorption and collaborative sensitization could be better understood. A natural start would be to investigate the dual dye system showing the current record power conversion efficiency [9].

Co-adsorbed dye systems are very complex. Pump-probe techniques, i.e. excitation by a light source (pump) followed by another light source to measure the excited system (probe), can be used to study fast processes in a system. From the solar cell perspective, this could be used to study the excited state of dye molecules and follow the charge transfer within the cell. These kinds of measurements need pulsed light sources with short pulses and have traditionally been performed using lasers for both pump and probe. Lately, the emergence of techniques using laser pump pulses and X-ray probes has made it possible to study both the valence region and the core levels of the excited system. These measurements could be performed at synchrotrons, X-ray free electron lasers (XFELs) or in a lab with a high-harmonic generation (HHG) source. Measurements of this kind could assist in understanding the complexity of the mixed systems.

The studies discussed above have all concerned the interface between dye and a mesoporous oxide substrate, i.e. not a complete DSC. Furthermore, all measurements have been performed in vacuum which is not the normal operating conditions of a DSC. Measurements under more realistic circumstances give valuable insights into the functional properties. This could be studied using high pressure (ambient pressure) PES, where the sensitized mesoporous oxide could be probed in the environment of the liquid electrolyte to include also solvation effects from the electrolyte.

The ultimate measurement, to really gain insight into these systems would be to include a solar simulator into the high pressure PES measurements and perform in operando measurements. Coupling the interfacial properties, obtained by PES, to the solar cell performance could increase the understanding of how the electronic and geometric surface structure affects the overall performance of the cell under operating conditions.

In short, also the future development of the DSC will require detailed knowledge of the interface at an atomic level. Samples where the mixture of dyes can be controlled together with the possibilities described above will contribute to this development in a way that is difficult with other techniques. For example by identifying structures that limit the power conversion process in ways similar to what has been introduced in the present thesis.

6. Svensk populärvetenskaplig sammanfattning

6.1 Energianvändning

Energiproduktionen i världen domineras av icke förnybara energikällor, främst fossila bränslen. Den globala energianvändningen ökar för varje år samtidigt som de fossila bränslelagren minskar. Dessutom medför användningen av fossila bränslen ökade utsläpp av växthusgaser, främst koldioxid. En ökad andel förnybar energiproduktion är ett måste för att klara av energiförsörjningen i framtiden. Förnybara energikällor (dit räknas vatten-, vind- och solkraft samt geotermisk energi) bidrar inte till utsläppen av koldioxid. Omkring 24 % av världens elektricitet kom från förnybara energikällor under 2015 [1]. I Sverige är läget ett annat än i stora delar av övriga världen. Kärn- och vattenkraft står vardera för ungefär 40 % av elektriciteten [4]. Vindkraft står för 7 % [4] medan solkraft enbart står för 0,06 % [4, 5], men nyinstallationen av solceller är hög. Siffrorna ovan avser endast produktionen av elektricitet. Fordonssektorns energiförbrukning, som domineras av fossila bränslen, är inte medräknad.

Varje år träffas jorden av 600 TW användbar energi från solen [2]. Det är ungefär 40 gånger mer än den årliga globala energikonsumtionen. Möjligheterna är således goda för att öka produktionen av solel. Energin från solljuset kan tas tillvara med hjälp av solceller. En solcell absorberar fotoner från solljuset och omvandlar energin direkt till elektrisk energi. Kiselbaserade solceller dominerar marknaden och kan ha en verkningsgrad på ca 25 %. Kostnaden för att tillverka kiselbaserade solceller har begränsat användningen. Under de senaste 25 åren har andra solcellstekniker, som andra halvledare, olika organiska solceller och färgämnessensiterade solceller utvecklats för att ta upp kampen mot kisel. Verkningsgraden hos dessa typer av solceller är lägre än för kiselbaserade solceller, men produktionskostnaden har potential att bli avsevärt lägre. I inomhusmiljöer, där ljusstyrkan är lägre och ljuset finns i ett annat våglängdsområde än utomhus, [8] har användningen av färgämnessensiterade solceller visat sig mycket lovande. Färgämnessensiterade solceller har en mycket högre verkningsgrad än andra typer av solceller vid inomhusbruk. Tänkbara användningsområden är bl.a. att integreras i laddare för olika elektroniska produkter, som t.ex. mobiltelefoner och surfplattor.

Arbetet som presenteras i denna avhandling kretsar kring förståelsen av gränsskikt i färgämnessensiterade solceller. Den ytkänsliga och elementspecifika metoden fotoelektronspektroskopi (PES) har använts för att studera aktiva gränsskikt i denna typ av solceller.

6.2 Färgämnessensiterade solceller

En artikel som publicerades 1991 visade att färgämnessensiterade solceller kan omvandla ljus till elektrisk energi med en verkningsgrad på omkring 7 % [7]. Sedan dess har intensiv forskning bedrivits och mängder av artiklar har publicerats [10]. Färgämnessensiterade solceller har en enkel struktur, vilket gör dem billiga att producera jämfört med andra typer av solceller. En färgämnessensiterad solcell innehåller två elektroder separerade med en redoxmediator som kan vara antingen en flytande elektrolyt eller ett fast hålledarmaterial. En majoritet av arbetet i denna avhandling rör färgämnessensiterade solceller med elektrolyt, vilket används i diskussionen nedan. En schematisk figur som visar en färgämnessensiterad solcell finns i Figur 6.1, där pilarna visar elektronöverföringar i cellen under belysning. I solcellen absorberas ljus vid den ena av elektroderna (arbetselektroden) genom att ett eller flera färgämnen som är adsorberade (bundna) till en mesoporös halvledarfilm absorberar fotoner. I denna avhandling har halvledarna titandioxid (TiO_2) och nickeloxid (NiO) studerats. Absorptionen av en foton gör att en elektron i färgämnet lyfts från grundtillståndet (F) till en högre nivå (F^*), varifrån den kan injiceras in i halvledaren. Färgämnet saknar nu en elektron och är positivt laddat, (F^+). Elektronen återfås från elektrolyten (E_{redox}) så att färgämnet återgår till grundtillståndet (F) igen och ljus kan åter absorberas. Från halvledaren leds elektronerna ut till en yttre krets där de kan utföra elektriskt arbete, för att sedan återföras till systemet genom den andra elektroden (motelektroden). Elektrolyten återfår elektroner från motelektroden, vilket sluter kretsen.

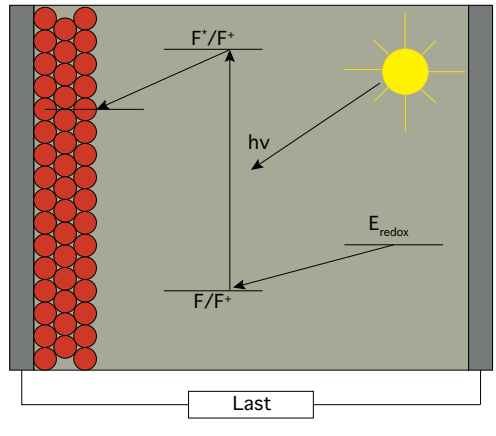

Figur 6.1. Schematisk illustration av en färgämnessensiterad solcell. Solen lyser på solcellen där färgämnet absorberar en foton, vilket leder till att en elektron exciteras till en högre nivå. Elektronen injiceras in i titandioxidfilmen (symboliserad av de röda bollarna) och leds ut i en krets där den kan utföra arbete. Färgämnet, som nu saknar en elektron, får tillbaka denna från elektrolyten och kan därmed åter absorbera en foton. Elektrolyten återfår elektroner från den yttre kretsen.

6.3 Fotoelektronspektroskopi

Fotoelektronspektroskopi (PES) är en elementspecifik metod med hög ytkänslighet. Ett prov belyses med röntgenstrålning med en känd energi, vilket frigör elektroner från provet. Genom att mäta den kinetiska energin hos de frigjorda elektronerna och veta fotonenergin kan elektronernas bindningsenergi i provet beräknas. Elektroner från varje energinivå (orbital) i varje element har en specifik bindningsenergi. Genom att beräkna bindningsenergin och räkna hur många elektroner som har en given energi kan ett spektrum erhållas. I Figur 6.2 visas processen schematiskt tillsammans med ett exempel på ett spektrum.

Röntgenstrålningen kan produceras på olika vis: labbkällor producerar röntgenstrålning med en specifik fotonenergi, medan synkrotroner ger strålning med varierbar fotonenergi.

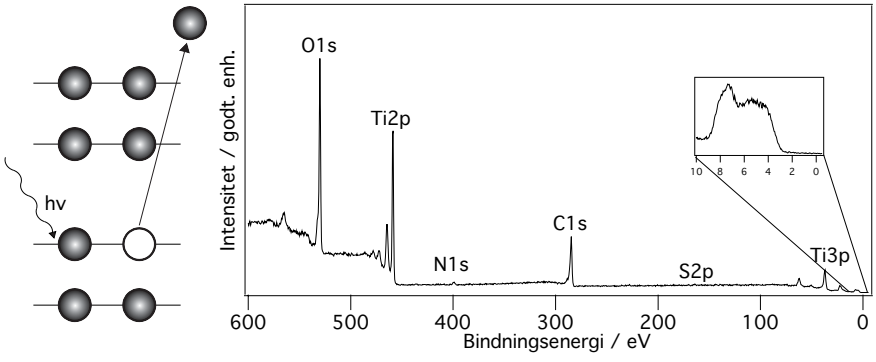

Figur 6.2. Figuren visar hur PES fungerar. T.v. en schematisk figur över principen bakom PES, där röntgenljus med känd energi, hν, infaller på provet och en elektron emitteras som en följd av detta. Energin på elektronen mäts och antalet elektroner för en given energi räknas för att erhålla ett spektrum. T.h. ett översiktsspektrum, som visar alla element som finns i provet, för färgämnet D35 på TiO_2 mätt med en fotonenergi på 758 eV.

6.4 Resultat

I arbetet som presenteras i denna avhandling har fotoelektronspektroskopi (PES) använts för att studera halvledare sensiterade med olika färgämnen. I Artikel I jämförs två färgämnen som trots snarlik kemisk struktur ger solceller med olika verkningsgrad. Inga skillnader upptäcks varken i hur färgämnena binder till titandioxiden eller i deras energinivåer. Däremot observeras skillnader i mängden färgämne på ytan. Skillnaden i verkningsgrad beror enbart på ytans geometri.

Färgämnen är generellt sett känsliga för värme, så i Artikel II undersöks hur två färgämnen påverkas av värmebehandling. Verkningsgraden sjunker med

mer än 90 % för båda och för det ena färgämnet ändras bindningen till titandioxiden. Detta leder till skiftade energinivåer och ökad rekombination, medan det andra färgämnet går sönder och delar av det lossnar när det värms.

Att kombinera färgämnen är ett sätt att öka ljusabsorptionen i en solcell. Artikel III och IV visar med hjälp av PES att två färgämnens bindning till titandioxiden ändras på ett sätt som är fördelaktigt för solcellsfunktionen när de kombineras med ett annat färgämne.

Artikel V jämför solceller baserade på titandioxid med olika morfologier. En ny morfologi som är lovande för fasta solceller ger högre spänning när den används i solceller. Med hjälp av PES visas att det beror på att det finns färre fällor i titandioxiden som elektroner kan fastna i efter att ha injicerats från färgämnet.

Solceller baserade på NiO har ofta problem med rekombination, vilket begränsar deras verkningsgrad. I Artikel VI visas att ett färgämnes bindning till nickeloxid kan ändras när det kombineras med en liten molekyl på ytan. Det får till följd att rekombinationen minskar och verkningsgraden ökar med en faktor 4.

Projekten har gett en ökad förståelse kring strukturer på ytan, både geometriska och elektroniska. PES har gett fördjupade insikter i hur färgämnen påverkas på molekylnivå när de kombineras med andra färgämnen och molekyler på en halvledaryta.

7. Acknowledgements

I would like to start by thanking my supervisors, Håkan Rensmo, Erik Johansson and Anders Hagfeldt. Håkan, you are the most pedagogical person I have ever met. Thank you for challenging me to make me learn more. Erik, thank you for always taking the time to discuss with me and explain things to me. Anders, thank you for always being positive and enthusiastic!

Thank you Hans Siegbahn for your invaluable input on manuscripts and the thesis.

Sareh, Ute, Maria, Anna and Hanna, thank you for the discussions on spectroscopy, solar cells and how to characterize them. It has meant a lot to me and has really contributed in a significant way.

A special thanks to Leif for preparing TiO_2 electrodes whenever I asked, even with short notice.

Thank you Stefan for teaching me about the ESCA and thank you Rein for your efforts in maintaining it. Thank you Rebecka for all the time spent together at synchrotrons, it has been fun! Thank you Josephina, Victor, Joachim, Davide, Olof, Christofer, Minjie and Dominik for the time together in the course lab. Kristofer, Meysam and Haining, thank you for good collaborations!

Thank you Anne and Inger for always helping me out with administrative questions. The staff at the MAX IV laboratory and BESSY are greatly acknowledged.

My gratitude of course also to all the past and present colleagues at Molecular and Condensed Matter Physics as well as within CMD.

Thank you Bertrand for sharing office with me and for our discussions on everything from science to sport.

Susanna, you were an excellent office mate and you are a good friend! Thank you for everything during these years!

To my family and friends: Thank you for all the support during these years. It has really meant a lot!

Elin, Sixten and Malte, this would not have been possible without you. Thank you and I love you!

References

[1] REN21. Renewables 2016 Global Status Report. Technical report, REN21 (2016).

[2] P Würfel. *Physics of Solar Cells - From Basic Principles to Advanced Concepts*. Wiley-VCH, second edition (2009).

[3] M. Grätzel. Photoelectrochemical Cells. *Nature*, **414**, 338–344 (2001).

[4] Energimyndigheten. Energiläget 2015. Technical report, Energimyndigheten (2015).

[5] J. Lindahl. National Survey Report of PV Power Applications in Sweden. Technical report, IEA-PVPS (2014).

[6] M. A. Green. *Solar Cells, Operating Principles, Technology and System Applications*. University of New South Wales, Australia (1998).

[7] B. O'Regan and M. Grätzel. A Low-Cost, High-Efficiency Solar Cell Based on Dye-Sensitized Colloidal TiO_2 Films. *Nature*, **353**, 737–740 (1991).

[8] N. Sridhar and D. Freeman. A Study of Dye Sensitized Solar Cells under Indoor and Low Level Outdoor Lighting: Comparison to Organic and Inorganic Thin Film Solar Cells and Methods to Address Maximum Power. *Conference Proceedings of the 26th EU-PVSEC*, pages 232–236 (2011).

[9] K. Kakiage, Y. Aoyama, T. Yano, K. Oya, J.-I. Fujisawa, and M. Hanaya. Highly-Efficient Dye-Sensitized Solar Cells with Collaborative Sensitization by Silyl-Anchor and Carboxy-Anchor Dyes. *Chem. Commun.*, **51**, 15894–15897 (2015).

[10] A. Hagfeldt, G. Boschloo, L. Sun, L. Kloo, and H. Pettersson. Dye-Sensitized Solar Cells. *Chem. Rev.*, **110**, 6595–6663 (2010).

[11] H. Tsubomura, M. Matsumura, Y. Nomura, and T. Amamiya. Dye Sensitised Zinc Oxide: Aqueous Electrolyte: Platinum Photocell. *Nature*, **261**, 402–403 (1976).

[12] R. Memming. Electorn Transfer Processes with Excited Molecules as Semiconductor Electrodes. *Progr. Surf. Sci.*, **17**, 7–74 (1984).

[13] J. Desilvestro, M. Grätzel, L. Kavan, J. Moser, and J. Augustynski. Highly Efficient Sensitization of Titanium Dioxide. *J. Am. Chem. Soc.*, **107**, 2988–2990 (1985).

[14] L. M. Peter. Dye-Sensitized Nanocrystalline Solar Cells. *Phys. Chem. Chem. Phys.*, **9**, 2630–2642 (2007).

[15] E. M. J. Johansson, R. Lindblad, H. Siegbahn, A. Hagfeldt, and H. Rensmo. Atomic and Electronic Structures of Interfaces in Dye-Sensitized, Nanostructured Solar Cells. *ChemPhysChem*, **15**, 1006–1017 (2014).

[16] J. Albero, P. Atienzar, A. Corma, and H. Garcia. Efficiency Records in Mesoscopic Dye-Sensitized Solar Cells. *Chem. Rec.*, **15**, 803–828 (2015).

[17] A. Yella, H.-W. Lee, H. N. Tsao, C. Yi, A. K. Chandiran, MD. K. Nazeeruddin, E. W.-G. Diau, C.-Y. Yeh, S. M. Zakeeruddin, and M. Grätzel. Porphyrin-Sensitized Solar Cells with Cobalt (II/III)-Based Redox Electrolyte Exceed 12 Percent Efficiency. *Science*, **334**, 629–634 (2011).

[18] S. Mathew, A. Yella, P. Gao, R. Humphry-Baker, B. F. E. Curchod, N. Ashari-Astani, I. Tavernelli, U. Rothlisberger, MD. K. Nazeeruddin, and M. Grätzel. Dye-Sensitized Solar Cells with 13% Efficiency Achieved Through the Molecular Engineering of Porphyrin Sensitizers. *Nature chemistry*, **6**, 242–247 (2014).

[19] F. Inakazu, Y. Noma, Y. Ogomi, and S. Hayase. Dye-Sensitized Solar Cells Consisting of Dye-Bilayer Structure Stained with Two Dyes for Harvesting Light of Wide Range of Wavelength. *Appl. Phys. Lett.*, **93**, 2–4 (2008).

[20] R. Y. Ogura, S. Nakane, M. Morooka, M. Orihashi, Y. Suzuki, and K. Noda. High-Performance Dye-Sensitized Solar Cell with a Multiple Dye System. *Appl. Phys. Lett.*, **94**, 1–3 (2009).

[21] Y. Ogomi, S. S. Pandey, S. Kimura, and S. Hayase. Probing Mechanism of Dye Double Layer Formation from Dye-Cocktail Solution for Dye-Sensitized Solar Cells. *Thin Solid Films*, **519**, 1087–1092 (2010).

[22] P. J. Holliman, M. Mohsen, A. Connell, M. L. Davies, K. Al-Salihi, M. B. Pitak, G. J. Tizzard, S. J. Coles, R. W. Harrington, W. Clegg, C. Serpa, O. H. Fontes, C. Charbonneau, and M. J. Carnie. Ultra-Fast Co-Sensitization and Tri-Sensitization of Dye-Sensitized Solar Cells with N719, SQ1 and Triarylamine Dyes. *J. Mater. Chem.*, **22**, 13318–13327 (2012).

[23] NREL. Best Research-Cell Efficiencies (April 2016).

[24] P. Atkins and J. de Paula. *Physical Chemistry*. Oxford University Press, 10th edition (2014).

[25] H. Ibach and H. Lüth. *Solid-State Physics - An Introduction to Principles of Materials Science*. Springer-Verlag, Berlin Heidelberg, 4th edition (2009).

[26] F.-T. Kong, S.-Y. Dai, and K.-J. Wang. Review of Recent Progress in Dye-Sensitized Solar Cells. *Adv. Optoelectron.*, **2007**, 1–13 (2007).

[27] T. W. Hamann, R. A. Jensen, A. B. F. Martinson, H. Van Ryswyk, and J. T. Hupp. Advancing Beyond Current Generation Dye-Sensitized Solar Cells. *Energy Environ. Sci.*, **1**, 66–78 (2008).

[28] M. Pagliaro, G. Palmisano, R. Ciriminna, and V. Loddo. Nanochemistry Aspects of Titania in Dye-Sensitized Solar Cells. *Energy Environ. Sci.*, **2**, 838–844 (2009).

[29] Q. Zhang, C. S. Dandeneau, X. Zhou, and G. Cao. ZnO Nanostructures for Dye-Sensitized Solar Cells. *Adv. Mater.*, **21**, 4087–4108 (2009).

[30] H. J. Snaith and C. Ducati. SnO_2-Based Dye-Sensitized Hybrid Solar Cells Exhibiting Near Unity Absorbed Photon-to-Electron Conversion Efficiency. *Nano Lett.*, **10**, 1259–1265 (2010).

[31] A. Stashans, S. Lunell, R. Bergström, A. Hagfeldt, and S. E. Lindquist. Theoretical Study of Lithium Intercalation in Rutile and Anatase. *Phys. Rev. B*, **53**, 159–170 (1996).

[32] D. Adler and J. Feinleib. Electrical and Optical Properties of Narrow Band Materials. *Phys. Rev. B*, **1693**, 3112–3134 (1970).

[33] B. Sasi, K. G. Gopchandran, P. K. Manoj, P. Koshy, P. Prabhakara Rao, and V. K. Vaidyan. Preparation of Transparent and Semiconducting NiO Films. *Vacuum*, **68**, 149–154 (2002).

[34] R. Palombari. Influence of Surface Acceptor-Donor Couples on Conductivity and other Electrochemical Properties of Nonstoichiometric NiO at 200 °C. *Journal of Electroanalytical Chemistry*, **546**, 23–28 (2003).

[35] B. Sasi and K. G. Gopchandran. Nanostructured Mesoporous Nickel Oxide Thin Films. *Nanotechnology*, **18**, 115613 (2007).

[36] J. Feinleib and D. Adler. Band Structure and Electrical Conductivity of NiO. *Phys. Rev. Lett.*, **21**, 1010–1013 (1968).

[37] G. A. Sawatzky and J. W. Allen. Magnitude and Origin of the Band Gap in NiO. *Phys. Rev. Lett.*, **53**, 2339–2342 (1984).

[38] R. Eder. Correlated Band Structure of NiO, CoO, and MnO by Variational Cluster Approximation. *Phys. Rev. B*, **78**, 1–15 (2008).

[39] V. Ponec, Z. Knor, and S. Černý. *Adsorption on Solids*. Butterworth & Co. (Publishers) Ltd. (1974).

[40] P. Hofmann. *Lecture Notes on Surface Science*, volume 2.5, Fall 2005. Århus University (2005).

[41] T. L. Hill. *An Introduction to Statistical Thermodynamics*. Dover Publications (1986).

[42] D. A. McQuarrie and J. D. Simon. *Physical Chemistry - A Molecular Approach*. University Science Books (1997).

[43] M. Khalfaoui, S. Knani, M. A. Hachicha, and A. Ben Lamine. New Theoretical Expressions for the Five Adsorption Type Isotherms Classified by BET Based on Statistical Physics Treatment. *J. Colloid Interface Sci.*, **263**, 350–356 (2003).

[44] P. Schneider. Adsorption Isotherms of Microporous-Mesoporous Solids Revisited. *Appl. Catal. A Gen.*, **129**, 157–165 (1995).

[45] J. Horniakova, M. Králik, A. Kaszonyi, and D. Mravec. A Practical Approach to the Treatment of Adsorption-Desorption Isotherms, Acidity and Catalytic Behaviour of Zeolite Catalysts. *Microporous Mesoporous Mater.*, **46**, 287–298 (2001).

[46] A. Mishra, M. K. R. Fischer, and P. Bäuerle. Metal-Free Organic Dyes for Dye-Sensitized Solar Cells: From Structure: Property Relationships to Design Rules. *Angew. Chem. Int. Ed.*, **48**, 2474–2499 (2009).

[47] W. Zeng, Y. Cao, Y. Bai, Y. Wang, Y. Shi, M. Zhang, F. Wang, C. Pan, and P. Wang. Efficient Dye-Sensitized Solar Cells with an Organic Photosensitizer Featuring Orderly Conjugated Ethylenedioxythiophene and Dithienosilole Blocks. *Chem. Mater.*, **22**, 1915–1925 (2010).

[48] D. P Hagberg, T. Marinado, K. M. Karlsson, K. Nonomura, P. Qin, G. Boschloo, T. Brinck, A. Hagfeldt, and L. Sun. Tuning the HOMO and LUMO Energy Levels of Organic Chromophores for Dye Sensitized Solar Cells. *J. Org. Chem.*, **72**, 9550–9556 (2007).

[49] S. M. Feldt, E. A. Gibson, E. Gabrielsson, L. Sun, G. Boschloo, and A. Hagfeldt. Design of Organic Dyes and Cobalt Polypyridine Redox Mediators for High-Efficiency Dye-Sensitized Solar Cells. *J. Am. Chem. Soc.*, **132**, 16714–16724 (2010).

[50] L. Kloo. On the Early Development of Organic Dyes for Dye-Sensitized Solar Cells. *Chem. Commun.*, **49**, 6580–6583 (2013).

[51] D. P. Hagberg, X. Jiang, E. Gabrielsson, M. Linder, T. Marinado, T. Brinck, A. Hagfeldt, and L. Sun. Symmetric and Unsymmetric Donor Functionalization. Comparing Structural and Spectral Benefits of Chromophores for Dye-Sensitized Solar Cells. *J. Mater. Chem.*, **19**, 7232–7238 (2009).

[52] H. Tian, E. Gabrielsson, P. W. Lohse, N. Vlachopoulos, L. Kloo, A. Hagfeldt, and L. Sun. Development of an Organic Redox Couple and Organic Dyes for Aqueous Dye-Sensitized Solar Cells. *Energy Environ. Sci.*, **5**, 9752–9755 (2012).

[53] E. Gabrielsson, H. Ellis, S. Feldt, H. Tian, G. Boschloo, A. Hagfeldt, and L. Sun. Convergent/Divergent Synthesis of a Linker-Varied Series of Dyes for Dye-Sensitized Solar Cells Based on the D35 Donor. *Adv. Energy Mater.*, **3**, 1647–1656 (2013).

[54] H. Ellis, S. K. Eriksson, S. M. Feldt, E. Gabrielsson, P. W. Lohse, R. Lindblad, L. Sun, H. Rensmo, G. Boschloo, and A. Hagfeldt. Linker Unit Modification of Triphenylamine-Based Organic Dyes for Efficient Cobalt Mediated Dye-Sensitized Solar Cells. *J. Phys. Chem. C*, **117**, 21029–21036 (2013).

[55] D. P. Hagberg, T. Edvinsson, T. Marinado, G. Boschloo, A. Hagfeldt, and L. Sun. A Novel Organic Chromophore for Dye-Sensitized Nanostructured Solar Cells. *Chem. Commun.*, pages 2245–2247 (2006).

[56] K. Westermark, S. Tingry, P. Persson, H. Rensmo, S. Lunell, A. Hagfeldt, and H. Siegbahn. Triarylamine on Nanocrystalline TiO_2 Studied in its Reduced and Oxidized State by Photoelectron Spectroscopy. *J. Phys. Chem. B*, **105**, 7182–7187 (2001).

[57] J. Nyhlen, G. Boschloo, A. Hagfeldt, L. Kloo, and T. Privalov. Regeneration of Oxidized Organic Photo-Sensitizers in Grätzel Solar Cells: Quantum-Chemical Portrait of a General Mechanism. *ChemPhysChem*, **11**, 1858–1862 (2010).

[58] MD. K. Nazeeruddin, A. Kay, I. Rodicio, R. Humphry-Baker, E. Mueller, P. Liska, N. Vlachopoulos, and M. Grätzel. Conversion of Light to Electricity by cis-X_2bis(2,2'-bipyridyl-4,4'-dicarboxylate)ruthenium(II) Charge-Transfer Sensitizers (X = Cl-, Br-, I-, CN-, and SCN-) on Nanocrystalline Titanium Dioxide Electrodes. *J. Am. Chem. Soc.*, **115**, 6382–6390 (1993).

[59] MD. K. Nazeeruddin, P. Péchy, and M. Grätzel. Efficient Panchromatic Sensitization of Nanocrystalline TiO_2 Films by a Black Dye Based on a Trithiocyanato-Ruthenium Complex. *Chem. Commun.*, **1**, 1705–1706 (1997).

[60] MD. K. Nazeeruddin, S. M. Zakeeruddin, R. Humphry-Baker, M. Jirousek, P. Liska, N. Vlachopoulos, V. Shklover, C.-H. Fischer, and M. Grätzel. Acid-Base Equilibria of (2,2'-Bipyridyl-4,4'-dicarboxylic acid)ruthenium(II) Complexes and the Effect of Protonation on Charge-Transfer Sensitization of Nanocrystalline Titania. *Inorg. Chem.*, **38**, 6298–6305 (1999).

[61] MD. K. Nazeeruddin, R. Humphry-Baker, P. Liska, and M. Grätzel. Investigation of Sensitizer Adsorption and the Influence of Protons on Current and Voltage of a Dye-Sensitized Nanocrystalline TiO_2 Solar Cell. *J. Phys. Chem. B*, **107**, 8981–8987 (2003).

[62] MD. K. Nazeeruddin, F. De Angelis, S. Fantacci, A. Selloni, G. Viscardi, P. Liska, S. Ito, B. Takeru, and M. Grätzel. Combined Experimental and DFT-TDDFT Computational Study of Photoelectrochemical Cell Ruthenium Sensitizers. *J. Am. Chem. Soc.*, **127**, 16835–16847 (2005).

[63] D. Kuang, C. Klein, S. Ito, J. E. Moser, R. Humphry-Baker, N. Evans, F. Duriaux, C. Grätzel, S. M. Zakeeruddin, and M. Grätzel. High-Efficiency and stable mesoscopic dye-sensitized solar cells based on a high molar extinction coefficient ruthenium sensitizer and nonvolatile electrolyte. *Adv. Mater.*, **19**, 1133–1137 (2007).

[64] P. Wang, S. M. Zakeeruddin, J. E. Moser, MD. K. Nazeeruddin, T. Sekiguchi, and M. Grätzel. A Stable quasi-Solid-State Dye-Sensitized Solar Cell with an Amphiphilic Ruthenium Sensitizer and Polymer Gel Electrolyte. *Nat. Mater.*, **2**, 402–407 (2003).

[65] E. M. J. Johansson, M. Hedlund, M. Odelius, H. Siegbahn, and H. Rensmo. Frontier Electronic Structures of Ru(tcterpy)$(NCS)_3$ and Ru(dcbpy)$_2(NCS)_2$: A Photoelectron Spectroscopy Study. *J. Chem. Phys.*, **126**, 244303 (2007).

[66] E. M. J. Johansson, M. Odelius, M. Gorgoi, O. Karis, R. Ovsyannikov, F. Schäfers, S. Svensson, H. Siegbahn, and H. Rensmo. Valence Electronic Structure of Ruthenium Based Complexes Probed by Photoelectron Spectroscopy at High Kinetic Energy (HIKE) and Modeled by DFT Calculations. *Chem. Phys. Lett.*, **464**, 192–197 (2008).

[67] E. M. J. Johansson, M. Odelius, S. Plogmaker, M. Gorgoi, S. Svensson, H. Siegbahn, and H. Rensmo. Spin - Orbit Coupling and Metal - Ligand Interactions in Fe (II), Ru (II), and Os (II) Complexes. *J. Phys. Chem. C*, **114**, 10314–10322 (2010).

[68] P. Persson, S. Lunell, P. A. Brühwiler, J. Schnadt, S. Södergren, J. N. O'Shea, O. Karis, H. Siegbahn, N. Mårtensson, M. Bässler, and L. Patthey. N1s X-ray Absorption Study of the Bonding Interaction of bi-isonicotinic Acid Adsorbed on Rutile TiO_2(110). *J. Chem. Phys.*, **112**, 3945–3948 (2000).

[69] K. Westermark, H. Rensmo, A. C. Lees, J. G. Vos, and H. Siegbahn. Electron Spectroscopic Studies of Ruthenium and Osmium Adsorbed on Nanostructured TiO_2 and ZnO Surfaces. *J. Phys. Chem. B*, **106**, 10108–10113 (2002).

[70] M. Hahlin. *Electronic and Molecular Surface Structures of Dye-Sensitized TiO_2 Interfaces*. PhD thesis, Uppsala university (2010).

[71] U. Bach, D. Lupo, P. Comte, J. E. Moser, F. Weissörtel, J. Salbeck, H. Spreitzer, and M. Grätzel. Solid-State Dye-Sensitized Mesoporous TiO_2 Solar Cells with High Photon-to-Electron Conversion Efficiencies. *Nature*, **395**, 583–585 (1998).

[72] M. A. Green, K. Emery, Y. Hishikawa, W. Warta, and E. D. Dunlop. Solar Cell Efficiency Tables (Version 47). *Prog. Photovoltaics*, **24**, 3–11 (2016).

[73] A. Hagfeldt and M. Grätzel. Light-Induced Redox Reactions in Nanocrystalline Systems. *Chem. Rev.*, **1**, 49–68 (1995).

[74] G. Boschloo, E. A. Gibson, and A. Hagfeldt. Photomodulated Voltammetry of Iiodide/Triiodide Redox Electrolytes and its Relevance to Dye-Sensitized Solar Cells. *J. Phys. Chem. Lett.*, **2**, 3016–3020 (2011).

[75] S. Cazzanti, S. Caramori, R. Argazzi, C. M. Elliott, and C. A. Bignozzi. Efficient Non-Corrosive Electron-Transfer Mediator Mixtures for Dye-Sensitized Solar Cells. *J. Am. Chem. Soc.*, **128**, 9996–9997 (2006).

[76] A. B. F. Martinson, T. W. Hamann, M. J. Pellin, and J. T. Hupp. New Architectures for Dye-Sensitized Solar Cells. *Chem. Eur. J.*, **14**, 4458–4467 (2008).

[77] S. Yanagida, Y. Yu, and K. Manseki. Iodine/Iodide-Free Dye-Sensitized Solar Cells. *Acc. Chem. Res.*, **42**, 1827–1838 (2009).

[78] S. Ardo and G. J. Meyer. Photodriven Heterogeneous Charge Transfer with Transition-Metal Compounds Anchored to TiO_2 Semiconductor Surfaces. *Chem. Soc. Rev.*, **38**, 115–164 (2009).

[79] A. Listorti, B. O'Regan, and J. R. Durrant. Electron Transfer Dynamics in Dye-Sensitized Solar Cells. *Chem. Mater.*, **23**, 3381–3399 (2011).

[80] W. Shockley and H. J. Queisser. Detailed Balance Limit of Efficiency of p-n Junction Solar Cells. *J. Appl. Phys.*, **32**, 510–519 (1961).

[81] A. Marti and G. L. Araujo. Limiting Efficiencies for Photovoltaic Energy Conversion in Multigap Systems. *Sol. Energ. Mat. Sol. C.*, **43**, 203–222 (1996).

[82] G. Conibeer. Third-Generation Photovoltaics. *Mater. Today*, **10**, 42–50 (2007).

[83] M. A. Green. *Third Generation Photovoltaics - Advanced Solar Energy Conversion*. Springer-Verlag, Berlin Heidelberg (2003).

[84] S. Hüfner. *Photoelectron spectroscopy - Principles and Applications*. Springer-Verlag, Berlin Heidelberg (2003).

[85] S. Suga and A. Sekiyama. *Photoelectron Spectroscopy - Bulk and Surface Electronic Structures*. Springer-Verlag, Berlin Heidelberg (2014).

[86] J. F. Moulder, W. F. Stickle, P. E. Sobol, and K. D. Bomben. *Handbook of X-ray Photoelectron Spectroscopy*. Physical Electronics Inc., Eden Prairie (1995).

[87] H. Siegbahn and L. Karlsson. *Photoelectron Spectroscopy*. Springer-Verlag, Berlin Heidelberg New York (1982).

[88] H. Hertz. Ueber einen Einfluss des ultravioletten Lichtes auf die electrische Entladung. *Ann. Phys.*, **267**, 983–1000 (1887).

[89] A. Einstein. Über einen die Erzeugung und Verwandlung des Lichtes betreffenden heuristischen Gesichtspunkt. *Ann. Phys.*, **322**, 132–148 (1905).

[90] K. M. Siegbahn, C. Nordling, A. Fahlman, R. Nordberg, K. Hamrin, J. Hedman, G. Johansson, T. Bergmark, S.-E. Karlsson, I. Lindgren, and B. Lindberg. *ESCA Atomic, Molecular and Solid State Structure Studied by Means of Electron Spectroscopy*. Almquist and Wiksells, Uppsala (1967).

[91] K. M. Siegbahn. Electron Spectroscopy for Atoms, Molecules and Condensed Matter. *Science*, **217**, 111–121 (1982).

[92] U. Gelius, E. Basilier, S. Svensson, T. Bergmark, and K. Siegbahn. A High Resolution ESCA Instrument with X-ray Monochromator for Gases and Solids. *J. Electron Spectrosc.*, **2**, 405–434 (1973).

[93] N. Mårtensson, P. Baltzer, P. A. Brühwiler, J.-O. Forsell, A. Nilsson, A. Stenborg, and B. Wannberg. A Very High Resolution Electron Spectrometer. *J. Electron Spectrosc.*, **70**, 117–128 (1994).

[94] J. J. Olivero and R. L. Longbothum. Empirical Fits to the Voigt Line Width: A Brief Review. *J. Quant. Spectrosc. Ra.*, **17**, 233–236 (1977).

[95] M. Bässler, J-.O. Forsell, O. Björneholm, R. Feifel, M. Jurvansuu, S. Aksela, S. Sundin, S. L. Sorensen, R. Nyholm, A. Ausmees, and S. Svensson. Soft

X-ray Undulator Beam Line I411 at MAX-II for Gases, Liquids and Solid Samples. *J. Electron Spectrosc.*, **101-103**, 953–957 (1999).

[96] M. Bässler, A. Ausmees, M. Jurvansuu, R. Feifel, J.-O. Forsell, P. de Tarso Fonseca, A. Kivimäki, S. Sundin, S. L. Sorensen, R. Nyholm, O. Björneholm, S. Aksela, and S. Svensson. Beam Line I411 at MAX II - Performance and First Results. *Nucl. Instrum. Meth. A*, **469**, 382–393 (2001).

[97] M. Gorgoi, S. Svensson, F. Schäfers, G. Öhrwall, M. Mertin, P. Bressler, O. Karis, H. Siegbahn, A. Sandell, H. Rensmo, W. Doherty, C. Jung, W. Braun, and W. Eberhardt. The High Kinetic Energy Photoelectron Spectroscopy Facility at BESSY Progress and First Results. *Nucl. Instrum. Meth. A*, **601**, 48–53 (2009).

[98] F. Schaefers, M. Mertin, and M. Gorgoi. KMC-1: A High Resolution and High Flux Soft X-ray Beamline at BESSY. *Rev. Sci. Instrum.*, **78**, 1–14 (2007).

[99] U. Gelius, B. Wannberg, P. Baltzer, H. Fellner-Feldegg, G. Carlsson, C.-G. Johansson, J. Larsson, P. Münger, and G. Vegerfors. A New ESCA Instrument with Improved Surface Sensitivity, Fast Imaging Properties and Excellent Energy Resolution. *J. Electron Spectrosc.*, **52**, 747–785 (1990).

[100] E. M. J. Johansson, M. Hedlund, H. Siegbahn, and H. Rensmo. Electronic and Molecular Surface Structure of Ru(tcterpy)$(NCS)_3$ and Ru(dcbpy)$_2(NCS)_2$ Adsorbed From Solution onto Nanostructured TiO_2: A Photoelectron Spectroscopy Study. *J. Phys. Chem. B*, **109**, 22256–22263 (2005).

[101] J. Stöhr. *NEXAFS Spectroscopy*. Number 25 in Springer Series in Surface Sciences. Springer-Verlag, Berlin Heidelberg (1992).

[102] W. Eberhardt, editor. *Applications of Synchrotron Radiation - High Resolution Studies of Molecules and Molecular Adsorbates on Surfaces*. Number 35 in Springer Series in Surface Sciences. Springer-Verlag, Berlin Heidelberg (1995).

[103] T. N. Murakami, N. Koumura, M. Kimura, and S. Mori. Structural Effect of Donor in Organic Dye on Recombination in Dye-Sensitized Solar Cells with Cobalt Complex Electrolyte. *Langmuir*, **30**, 2274–2279 (2014).

[104] Z. S. Wang, N. Koumura, Y. Cui, M. Takahashi, H. Sekiguchi, A. Mori, T. Kubo, A. Furube, and K. Hara. Hexylthiophene-Functionalized Carbazole Dyes for Efficient Molecular Photovoltaics: Tuning of Solar-Cell Performance by Structural Modification. *Chem. Mater.*, **20**, 3993–4003 (2008).

[105] H. Pettersson, T. Gruszecki, L. H. Johansson, and P. Johander. Manufacturing Method for Monolithic Dye-Sensitised Solar Cells Permitting Long-Term Stable Low-Power Modules. *Sol. Energ. Mat. Sol. C.*, **77**, 405–413 (2003).

[106] M. Toivola, T. Peltola, K. Miettunen, J. Halme, and P. Lund. Thin Film Nano Solar Cells - From Device Optimization to Upscaling. *J. Nanosci. Nanotechnol.*, **10**, 1078–1084 (2010).

[107] A. Mathew, G. Mohan Rao, and N. Munichandraiah. Towards Fabrication of Stable Dye Sensitized Solar Cells Based on Acetonitrile as Solvent for the Redox Couple. *Adv. Mat. Lett.*, **5**, 180–183 (2014).

[108] K. Fredin, E. M. J. Johansson, T. Blom, M. Hedlund, K. Leifer, and H. Rensmo. Using a Molten Organic Conducting Material to Infiltrate a Nanoporous Semiconductor Film and its use in Solid-State Dye-Sensitized Solar Cells. *Synthetic Met.*, **159**, 166–170 (2009).

[109] M. Shima, M. Isomura, K. I. Wakisaka, K. Murata, and M. Tanaka. The Influence of Operation Temperature on the Output Properties of Amorphous Silicon-Related Solar Cells. *Sol. Energ. Mat. Sol. C.*, **85**, 167–175 (2005).

[110] S. R. Raga and F. Fabregat-Santiago. Temperature Effects in Dye-Sensitized Solar Cells. *Phys. Chem. Chem. Phys.*, **15**, 2328–2336 (2013).

[111] K. Fredin, K. F. Anderson, N. W. Duffy, G. J. Wilson, C. J. Fell, D. P. Hagberg, L. Sun, U. Bach, and S. E. Lindquist. Effect on Cell Efficiency Following Thermal Degradation of Dye-Sensitized Mesoporous Electrodes using N719 and D5 Sensitizers. *J. Phys. Chem. C*, **113**, 18902–18906 (2009).

[112] P. Tuyet Nguyen, R. Degn, H. Thai Nguyen, and T. Lund. Thiocyanate Ligand Substitution Kinetics of the Solar Cell Dye Z-907 by 3-methoxypropionitrile and 4-*tert*-butylpyridine at Elevated Temperatures. *Sol. Energ. Mat. Sol. C.*, **93**, 1939–1945 (2009).

[113] H. Thai Nguyen, H. M. Ta, and T. Lund. Thermal Thiocyanate Ligand Substitution Kinetics of the Solar Cell Dye N719 by Acetonitrile, 3-methoxypropionitrile, and 4-*tert*-butylpyridine. *Sol. Energ. Mat. Sol. C.*, **91**, 1934–1942 (2007).

[114] D. Bari, N. Wrachien, R. Tagliaferro, S. Penna, T. M. Brown, A. Reale, A. Di Carlo, G. Meneghesso, and A. Cester. Thermal Stress Effects on Dye-Sensitized Solar Cells (DSSCs). *Microelectron. Reliab.*, **51**, 1762–1766 (2011).

[115] Y. Mee Jung, Y. Park, S. Sarker, J.-J. Lee, U. Dembereldorj, and S.-W. Joo. Surface-Induced Thermal Decomposition of $[Ru(dcbpyH)_2\text{-}(CN)_2]$ on Nanocrystalline TiO_2 Surfaces: Temperature-Dependent Infrared Spectroscopy and Two-Dimensional Correlation Analysis. *Sol. Energ. Mat. Sol. C.*, **95**, 326–331 (2011).

[116] C.H. Law, R. Spence, and B. C. O'Regan. Brief Air Heating of TiO_2/Dye Films, to 120–250 °C; the Effect on Resulting Liquid Junction Dye Sensitised Solar Cells (DSSCs) and Melt-Processed Solid-State DSSCs. *J. Mater. Chem. A*, **1**, 14154–14161 (2013).

[117] M. Hahlin, E. M. J. Johansson, S. Plogmaker, M. Odelius, D. P. Hagberg, L. Sun, H. Siegbahn, and H. Rensmo. Electronic and Molecular Structures of Organic Dye/TiO_2 Interfaces for Solar Cell Applications: A Core Level Photoelectron Spectroscopy Study. *Phys. Chem. Chem. Phys.*, **12**, 1507–1517 (2010).

[118] M. Hahlin, E. M. J. Johansson, R. Schölin, H. Siegbahn, and H. Rensmo. Influence of Water on the Electronic and Molecular Surface Structures of Ru-Dyes at Nanostructured TiO_2. *J. Phys. Chem. C*, **115**, 11996–12004 (2011).

[119] S. Chaturvedi, J. A. Rodriguez, T. Jirsak, and J. Hrbek. Surface Chemistry of SO_2 on Zn and ZnO: Photoemission and Molecular Orbital Studies. *J. Phys. Chem. B*, **102**, 7033–7043 (1998).

[120] J. A. Rodriguez, T. Jirsak, S. Chaturvedi, and M. Kuhn. Reaction of SO_2 with ZnO(0001)-O and ZnO Powders: Photoemission and XANES Studies on the Formation of SO_3 and SO_4. *Surf. Sci.*, **442**, 400–412 (1999).

[121] J. A. Rodriguez, J. Hrbek, Z. Chang, J. Dvorak, T. Jirsak, and A. Maiti. Importance of O Vacancies in the Behavior of Oxide Surfaces: Adsorption of Sulfur on TiO_2 (110). *Phys. Rev. B*, **65**, 235414 (2002).

[122] D. Stoltz, A. Önsten, U. O. Karlsson, and M. Göthelid. High Resolution Spectroscopic and Microscopic Signatures of Ordered Growth of Ferrous Sulfate in SO_2 Assisted Corrosion of Fe_3O_4 (100). *Appl. Phys. Lett.*, **91**, 93107 (2007).

[123] S. K. Eriksson, I. Josefsson, H. Ellis, A. Amat, M. Pastore, J. Oscarsson, R. Lindblad, A. I. K. Eriksson, E. M. J. Johansson, G. Boschloo, A. Hagfeldt, S. Fantacci, M. Odelius, and H. Rensmo. Geometrical and Energetical Structural Changes in Organic Dyes for Dye-Sensitized Solar Cells Probed Using Photoelectron Spectroscopy and DFT. *Phys. Chem. Chem. Phys.*, **18**, 252–260 (2016).

[124] Y. Chiba, A. Islam, Y. Watanabe, R. Komiya, N. Koide, and L. Han. Dye-Sensitized Solar Cells with Conversion Efficiency of 11.1%. *Jpn. J. Appl. Phys.*, **45**, L638–L640 (2006).

[125] M. Wang, X. Li, H. Lin, P. Pechy, S. M. Zakeeruddin, and M. Grätzel. Passivation of Nanocrystalline TiO_2 Junctions by Surface Adsorbed Phosphinate Amphiphiles Enhances the Photovoltaic Performance of Dye Sensitized Solar Cells. *Dalton Trans.*, pages 10015–10020 (2009).

[126] P. Wang, S. M. Zakeeruddin, P. Comte, R. Charvet, R. Humphry-Baker, and M. Grätzel. Enhance the Performance of Dye-Sensitized Solar Cells by Co-grafting Amphiphilic Sensitizer and Hexadecylmalonic Acid on TiO_2 Nanocrystals. *J. Phys. Chem. B*, **107**, 14336–14341 (2003).

[127] P. Wang, S. M. Zakeeruddin, R. Humphry-Baker, J. E. Moser, and M. Grätzel. Molecular-Scale Interface Engineering of TiO_2 Nanocrystals: Improve the Efficiency and Stability of Dye-Sensitized Solar Cells. *Adv. Mater.*, **15**, 2101–2104 (2003).

[128] P. Wang, C. Klein, R. Humphry-Baker, S. M. Zakeeruddin, and M. Grätzel. Stable 8 % Efficient Nanocrystalline Dye-Sensitized Solar Cell Based on an Electrolyte of Low Volatility. *Appl. Phys. Lett.*, **86**, 1–3 (2005).

[129] N. R. Neale, N. Kopidakis, J. van de Lagemaat, M. Grätzel, and A. J. Frank. Effect of a Coadsorbent on the Performance of Dye-Sensitized TiO_2 Solar Cells: Shielding versus Band-Edge Movement. *J. Phys. Chem. B*, **109**, 23183–23189 (2005).

[130] Z. Zhang, S. M. Zakeeruddin, B. C. O'Regan, R. Humphry-Baker, and M. Grätzel. Influence of 4-Guanidinobutyric Acid as Coadsorbent in Reducing Recombination in Dye-Sensitized Solar Cells. *J. Phys. Chem. B*, **109**, 21818–21824 (2005).

[131] Z. Zhang, N. Evans, S. M. Zakeeruddin, R. Humphry-Baker, and M. Grätzel. Effects of ω-Guanidinoalkyl Acids as Coadsorbents in Dye-Sensitized Solar Cells. *J. Phys. Chem. C*, **111**, 398–403 (2007).

[132] K. Hara, Y. Dan-oh, C. Kasada, Y. Ohga, A. Shinpo, S. Suga, K. Sayama, and H. Arakawa. Effect of Additives on the Photovoltaic Performance of Coumarin-Dye-Sensitized Nanocrystalline TiO_2 Solar Cells. *Langmuir*, **20**, 4205–4210 (2004).

[133] X. Li, H. Lin, S. M. Zakeeruddin, M. Grätzel, and J. Li. Interface Modification of Dye-sensitized Solar Cells with Pivalic Acid to Enhance the Open-circuit Voltage. *Chem. Lett.*, **38**, 322–323 (2009).

[134] Z. S. Wang, Y. Cui, Y. Dan-oh, C. Kasada, A. Shinpo, and K. Hara. Thiophene-Functionalized Coumarin Dye for Efficient Dye-Sensitized Solar Cells: Electron Lifetime Improved by Coadsorption of Deoxycholic Acid. *J. Phys. Chem. C*, **111**, 7224–7230 (2007).

[135] K. Sayama, S. Tsukagoshi, T. Mori, K. Hara, Y. Ohga, A. Shinpou, Y. Abe, S. Suga, and H. Arakawa. Efficient Sensitization of Nanocrystalline TiO_2 Films with Cyanine and Merocyanine Organic Dyes. *Sol. Energ. Mat. Sol. C.*, **80**, 47–71 (2003).

[136] A. Kay and M. Grätzel. Artificial Photosynthesis. 1. Photosensitization of Titania Solar Cells with Chlorophyll Derivatives and Related Natural Porphyrins. *J. Phys. Chem.*, **97**, 6272–6277 (1993).

[137] K. Hara, T. Sato, R. Katoh, A. Furube, Y. Ohga, A. Shinpo, S. Suga, K. Sayama, H. Sugihara, and H. Arakawa. Molecular Design of Coumarin Dyes for Efficient Dye-Sensitized Solar Cells. *J. Phys. Chem. B*, **107**, 597–606 (2003).

[138] K. Hara, Z. S. Wang, T. Sato, A. Furube, R. Katoh, H. Sugihara, Y. Dan-oh, C. Kasada, A. Shinpo, and S. Suga. Oligothiophene-Containing Coumarin Dyes for Efficient Dye-Sensitized Solar Cells. *J. Phys. Chem. B*, **109**, 15476–15482 (2005).

[139] J. Lim, Y. S. Kwon, and T. Park. Effect of Coadsorbent Properties on the Photovoltaic Performance of Dye-Sensitized Solar Cells. *Chem. Commun.*, **47**, 4147–4149 (2011).

[140] H. Shen, H. Lin, Y. Liu, X. Li, J. Zhang, N. Wang, and J. Li. A Novel Diphenylphosphinic Acid Coadsorbent for Dye-Sensitized Solar Cell.

Electrochim. Acta, **56**, 2092–2097 (2011).

[141] L. Han, A. Islam, H. Chen, C. Malapaka, B. Chiranjeevi, S. Zhang, X. Yang, and M. Yanagida. High-Efficiency Dye-Sensitized Solar Cell with a Novel Co-Adsorbent. *Energy Environ. Sci.*, **5**, 6057–6060 (2012).

[142] K. M. Lee, C. Y. Chen, S. J. Wu, S. C. Chen, and C. G. Wu. Surface Passivation: The Effects of CDCA Co-Adsorbent and Dye Bath Solvent on the Durability of Dye-Sensitized Solar Cells. *Sol. Energ. Mat. Sol. C.*, **108**, 70–77 (2013).

[143] P. Chen, J. Brillet, H. Bala, P. Wang, S. M. Zakeeruddin, and M. Grätzel. Solid-State Dye-Sensitized Solar Cells using TiO_2 Nanotube Arrays on FTO Glass. *J. Mater. Chem.*, **19**, 5325–5328 (2009).

[144] M. Wang, J. Bai, F. Le Formal, S.-J. Moon, L. Cevey-Ha, R. Humphry-Baker, C. Grätzel, S. M. Zakeeruddin, and M. Grätzel. Solid-State Dye-Sensitized Solar Cells using Ordered TiO_2 Nanorods on Transparent Conductive Oxide as Photoanodes. *J. Phys. Chem. C*, **116**, 3266–3273 (2012).

[145] E. J. W. Crossland, N. Noel, V. Sivaram, T. Leijtens, J. A. Alexander-Webber, and H. J. Snaith. Mesoporous TiO_2 Single Crystals Delivering Enhanced Mobility and Optoelectronic Device Performance. *Nature*, **495**, 215–219 (2013).

[146] D. Chen, F. Huang, Y. B. Cheng, and R. A. Caruso. Mesoporous Anatase TiO_2 Beads with High Surface Areas and Controllable Pore Sizes: A Superior Candidate for High-Performance Dye-Sensitized Solar Cells. *Adv. Mater.*, **21**, 2206–2210 (2009).

[147] F. Sauvage, D. Chen, P. Comte, F. Huang, L.-P. Heiniger, Y. B. Cheng, R. A. Caruso, and M. Grätzel. Dye-Sensitized Solar Cells Employing a Single Film of Mesoporous TiO_2 Beads Achieve Power Conversion Efficiencies Over 10%. *ACS Nano*, **4**, 4420–4425 (2010).

[148] M. Pazoki, N. Taghavinia, A. Hagfeldt, and G. Boschloo. Mesoporous TiO_2 Microbead Electrodes for Cobalt-Mediator-Based Dye-Sensitized Solar Cells. *J. Phys. Chem. C*, **118**, 16472–16478 (2014).

[149] P. Qin, J. Wiberg, E. A. Gibson, M. Linder, L. Li, T. Brinck, A. Hagfeldt, B. Albinsson, and L. Sun. Synthesis and Mechanistic Studies of Organic Chromophores with Different Energy Levels for p-Type Dye-Sensitized Solar Cells. *J. Phys. Chem. C*, **114**, 4738–4748 (2010).

[150] A. Nattestad, A. J. Mozer, M. K. R. Fischer, Y. B. Cheng, A. Mishra, P. Bäuerle, and U. Bach. Highly Efficient Photocathodes for Dye-Sensitized Tandem Solar Cells. *Nat. Mater.*, **9**, 31–35 (2010).

[151] Z. Ji, G. Natu, Z. Huang, O. Kokhan, X. Zhang, and Y. Wu. Synthesis, Photophysics, and Photovoltaic Studies of Ruthenium Cyclometalated Complexes as Sensitizers for p-type NiO Dye-Sensitized Solar Cells. *J. Phys. Chem. C*, **116**, 16854–16863 (2012).

[152] T. Bessho, S. M. Zakeeruddin, C.-Y. Yeh, E. W.-G. Diau, and M. Grätzel. Highly Efficient Mesoscopic Dye-Sensitized Solar Cells based on Donor-Acceptor-Substituted Porphyrins. *Angew. Chem. Int. Ed.*, **49**, 6646–6649 (2010).

[153] H. Yamada, H. Imahori, Y. Nishimura, I. Yamazaki, and S. Fukuzumi. Enhancement of Photocurrent Generation by ITO Electrodes Modified Chemically with Self-Assembled Monolayers of Porphyrin-Fullerene Dyads. *Adv. Mater.*, **14**, 892–895 (2002).

[154] H. Yamada, H. Imahori, Y. Nishimura, I. Yamazaki, T. K. Ahn, S. K. Kim, D. Kim, and S. Fukuzumi. Photovoltaic Properties of Self-Assembled Monolayers of Porphyrins and Porphyrin-Fullerene Dyads on ITO and Gold Surfaces. *J. Am. Chem. Soc.*, **125**, 9129–9139 (2003).

[155] S. Xiao, Y. Li, Y. Li, J. Zhuang, N. Wang, H. Liu, B. Ning, Y. Liu, F. Lu, L. Fan, C. Yang, Y. Li, and D. Zhu. [60]Fullerene-Based Molecular Triads with Expanded Absorptions in the Visible Region: Synthesis and Photovoltaic Properties. *J. Phys. Chem. B*, **108**, 16677–16685 (2004).

[156] H. Imahori and S. Fukuzumi. Porphyrin-and Fullerene-Based Molecular Photovoltaic Devices. *Adv. Funct. Mater.*, **14**, 525–536 (2004).

[157] A. Takai, M. Chkounda, A. Eggenspiller, C. P. Gros, M. Lachkar, J. M. Barbe, and S. Fukuzumi. Efficient Photoinduced Electron Transfer in a Porphyrin Tripod-Fullerene Supramolecular Complex via π - π Interactions in Nonpolar Media. *J. Am. Chem. Soc.*, **132**, 4477–4489 (2010).

[158] C. S. Gopinath, R. P. Pandian, and P. T. Manoharan. Electronic Structure of Thiaporphyrins: An X-ray Photoelectron Spectroscopic Study. *J. Chem. Soc. Dalton Trans.*, pages 1255–1259 (1996).

[159] A. Rienzo, L. C. Mayor, G. Magnano, C. J. Satterley, E. Ataman, J. Schnadt, K. Schulte, and J. N. O'Shea. X-ray Absorption and Photoemission Spectroscopy of Zinc Protoporphyrin Adsorbed on Rutile TiO_2 (110) Prepared by In Situ Electrospray Deposition. *J. Chem. Phys.*, **132**, 084703 (2010).

[160] V. N. Nemykin, P. Galloni, B. Floris, C. D. Barrett, R. G. Hadt, R. I. Subbotin, A. G. Marrani, R. Zanoni, and N. M. Loim. Metal-Free and Transition-Metal Tetraferrocenylporphyrins Part 1: Synthesis, Characterization, Electronic Structure, and Conformational Flexibility of Neutral Compounds. *Dalton Trans.*, pages 4233–4246 (2008).

Acta Universitatis Upsaliensis

Digital Comprehensive Summaries of Uppsala Dissertations from the Faculty of Science and Technology 1409

Editor: The Dean of the Faculty of Science and Technology

A doctoral dissertation from the Faculty of Science and Technology, Uppsala University, is usually a summary of a number of papers. A few copies of the complete dissertation are kept at major Swedish research libraries, while the summary alone is distributed internationally through the series Digital Comprehensive Summaries of Uppsala Dissertations from the Faculty of Science and Technology. (Prior to January, 2005, the series was published under the title "Comprehensive Summaries of Uppsala Dissertations from the Faculty of Science and Technology".)

Distribution: publications.uu.se
urn:nbn:se:uu:diva-301164

ACTA
UNIVERSITATIS
UPSALIENSIS
UPPSALA
2016